Low-cost hydrocarbon membrane enables commercial-scale alkaline-based flow batteries for long-duration energy storage

Zhizhang Yuan[1,5], Lixin Liang[2,3,5], Qing Dai[1,3], Tianyu Li[1], Qilei Song[4], Huamin Zhang[1], Guangjin Hou[2] and Xianfeng Li[1]*

[1]Division of Energy Storage, Dalian National Laboratory for Clean Energy (DNL), Dalian Institute of Chemical Physics, Chinese Academy of Sciences, Dalian, China.
[2]State Key Laboratory of Catalysis, Dalian National Laboratory for Clean Energy (DNL), Dalian Institute of Chemical Physics, Chinese Academy of Sciences, Dalian, China.
[3]University of Chinese Academy of Sciences, Beijing, China.
[4]Barrer Centre, Department of Chemical Engineering, Imperial College London, London, UK.
[5]These authors contributed equally: Zhizhang Yuan and Lixin Liang.
*Correspondence to: X. F. Li (lixianfeng@dicp.ac.cn)

Abstract: Flow batteries are promising for long-duration grid-scale energy storage. Future terawatt-scale deployment of flow batteries will require substantial capital cost reduction, particularly low-cost electrolytes and hydrocarbon ion exchange membranes. However, integration of hydrocarbon membranes with novel flow battery chemistries in commercial-scale stacks is yet to be demonstrated. Here we report the pilot scale synthesis and roll-to-roll manufacturing of sulfonated poly(ether ether ketone) (SPEEK) membranes and demonstrate their high hydroxide conductivity and chemical stability in kW-scale alkaline-based flow batteries. After exposure to a 5 mol L^{-1} NaOH solution at 60 °C for 41 days, the SPEEK membrane still enabled a stable alkaline zinc-iron flow battery performance for more than 650 cycles (more than 650 hours) at high current densities (80 to 160 mA cm^{-2}). Furthermore, the membrane was integrated in flow battery stacks with power up to 4000 W, which demonstrated a high energy efficiency of 85.5% operated at 80 mA cm^{-2} and long term stable operation over 800 h as well as substantial cost savings relative to Nafion membranes. This work illustrates a potential pathway for manufacturing and upscaling of next-generation cost-effective flow batteries based on low-cost hydrocarbon membranes developed in past decades to translate to large scale applications for long-duration energy storage.

Introduction

With the rapid development of renewable energy such as solar and wind power, there is an urgent need for electrochemical energy conversion and storage technologies[1-6], such as flow batteries, electrolyzers, and fuel cells. In these electrochemical devices, membrane is a critical component that isolates the electrolytes as well as conducts charge carriers to complete the internal circuit[7,8]. Membranes with high hydroxide (OH^-) conductivity and stability in alkaline media are desirable for next-generation electrochemical energy conversion and storage devices, such as alkaline zinc-iron flow batteries[9,10] (Fig. 1a) and organic redox flow batteries[11,12] (Fig. 1b), and anion-exchange membrane water electrolysers[13]. An ideal membrane should have high stability in alkaline media and high selectivity for the target species. Nearly all of the commercially available membranes are based on perfluorosulfonic acid (PFSA), such as Nafion developed by DuPont (Fig. 1c)[14]. However, the high cost of Nafion membranes ($500 m^{-2}) accounts to up to 50% of capital costs of flow battery stacks[15,16], which limits the large scale application of electrochemical technologies. Furthermore, there are growing concerns about environmental impacts of Nafion manufacturing and the by-products perfluoroalkyl and polyfluoroalkyl substances (PFAS), known as “forever chemicals”, which can cause contamination of drinking water and pose long-term threats to human health. The Terawatt-scale renewable energy conversion and storage will require millions of meter square ion exchange membranes. Therefore, there is an urgent need to replace the Nafion membranes with alternative sustainable membranes with substantial cost reduction[17,18].

This preprint research paper has not been peer reviewed. Electronic copy available at: https://ssrn.com/abstract=3981895

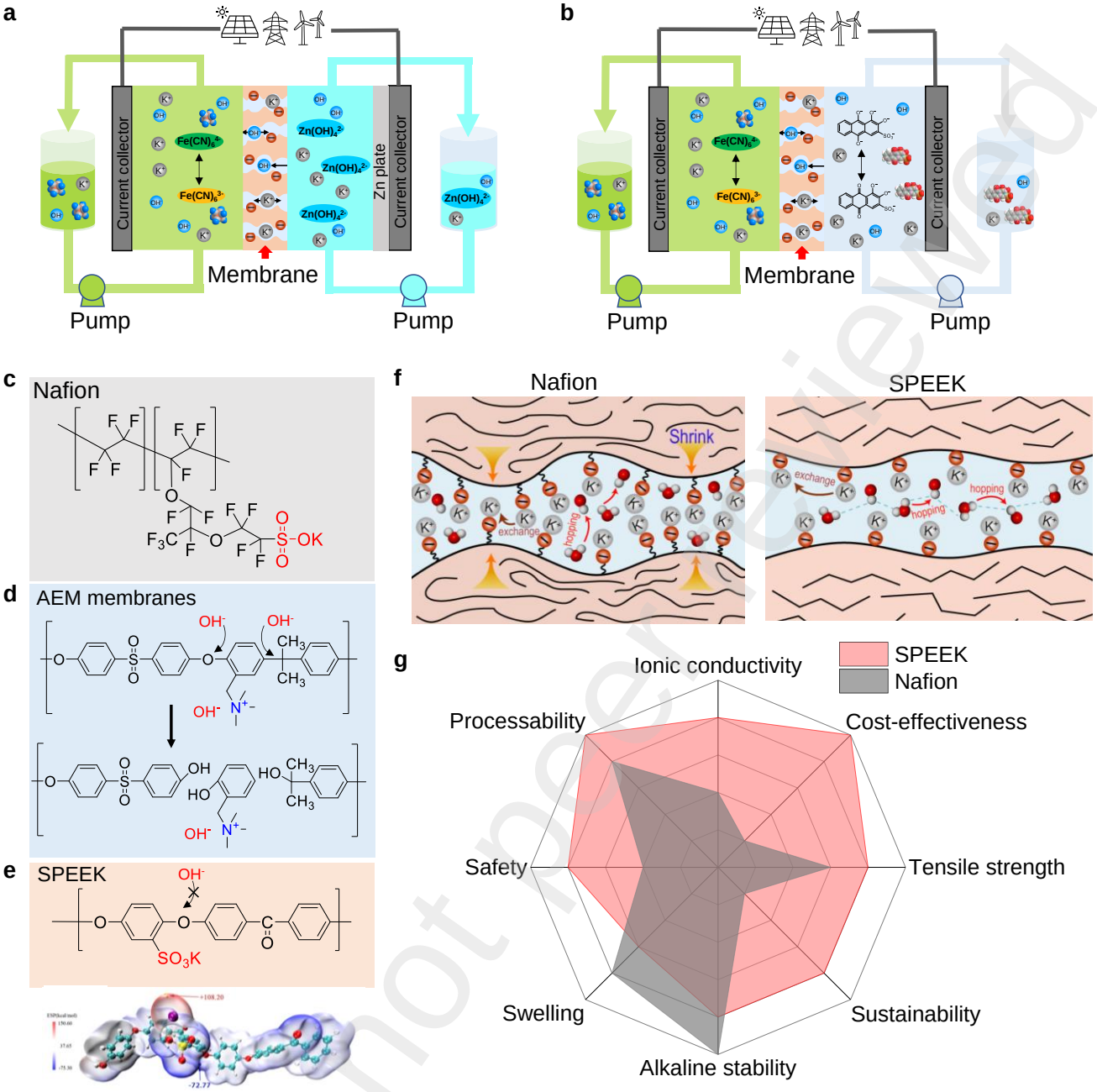


Fig. 1 Membranes in electrochemical energy conversion and storage technologies. The applications of membrane in **a**, alkaline zinc-iron flow battery and **b**, alkaline quinone-iron flow battery. **c**, Structure of Nafion. **d**, Degradation of hydrocarbon ion exchange membranes in alkaline media. **e**, Chemical structure and electrostatic potential (ESP) on an isosurface of electronic density (0.001 a.u.) for SPEEK. **f**, Schematic diagram for ion transport behaviors of Nafion and SPEEK membranes in alkaline media. **g**, Ranking of key performance indicators for SPEEK and Nafion membranes.

Non-fluorinated hydrocarbon ion exchange membranes exhibit significant advantages over PFSA membranes in terms of technical performance, cost, and environmental impacts. In the past three to four decades, significant efforts have been made to develop hydrocarbon-based ion exchange membranes[19], including cation-exchange membranes and anion-exchange membranes[20] for flow batteries and fuel cells[20-23]. The stability of hydrocarbon-based anion-exchange membranes is strongly dependent on the intrinsic features of the cationic groups. Extensive studies have shown that hydroxide ions can easily attack the polymer backbone and anion-exchange groups,

This preprint research paper has not been peer reviewed. Electronic copy available at: https://ssrn.com/abstract=3981895

leading to degradation through nucleophilic substitution[20,23,24], Hofmann elimination reaction or chemical rearrangement (e.g., Sommelet-Hauser and Stevens rearrangement)[25]. For example, a quaternary ammonium group holding a OH^- counter anion is an electron-withdrawing group and can trigger degradation of the polysulfone backbone (Fig. 1d)[24]. Cation-exchange membranes with anion groups are capable of transporting cations in alkaline media (i.e. anionic groups with associated K^+ or Na^+ counter cations). Nevertheless, cation-exchange membranes, with the exception of Nafion (Supplementary information Table 1)[9,26], are rarely applied in alkaline-based systems since cations (K^+ or Na^+) are their main charge carriers, which in turn result in membranes with a low ionic conductivity in alkaline media. To date, there are relatively few attempts to apply hydrocarbon-based cation-exchange membranes in novel alkaline battery systems in laboratory scale[22,27,28] however, the long term stability and performance remain to be improved. To the best of our knowledge, large scale demonstrations of low-cost hydrocarbon membranes and integration with novel flow battery chemistries in commercial-scale battery stacks have not been reported.

Herein, we report the pilot-scale synthesis and roll-to-roll manufacturing of sulfonated poly(ether-ether-ketone) (SPEEK) and demonstrated their superior performance and long-term stability in kW-scale alkaline zin-iron redox flow batteries. By carefully controlling the sulfonation modification, we obtained SPEEK membrane with reasonable ion exchange capacity. Although SPEEK membranes have been extensively studied as proton-conductive membranes in fuel cells, for the first time, our work reports the fast transport of hydroxide ions in alkaline electrolytes and fundamental understanding of the mechanisms. The rigid polymer chains (Fig. 1e), coupled with the weak charge properties from the skeleton and the dispersive cation-exchange groups (Fig. 1e), induces the formation of continuous hydrogen-bonding networks which favor the transport of OH^- ions through a Grotthuss mechanism (Fig. 1f), thus providing a high OH^- conductivity in SPEEK, as indicated by nuclear magnetic resonance (NMR) spectroscopy. The electronegative framework of cation-exchange membranes limits the attack from OH^-, which endow the membrane with an excellent stability in alkaline media. We demonstrate the superior performance of SPEEK membrane in alkaline zinc-iron flow battery (AZIFB) single cells and kW-scale cell stacks, showing high energy efficiency and high cycling stability up to 800 h. Comparison of key performance indicators suggests that the low-cost hydrocarbon membrane is a promising alternative to benchmark Nafion membranes (Fig. 1g, the key parameters for this ranking were given in Supplementary information Table 2). Our work bridged the gap between laboratory scale development of battery components and industrial scale flow battery stack operation, which will inspire the development of next-generation cost-effective flow batteries based on low-cost hydrocarbon membranes for large scale electrochemical energy storage applications.

This preprint research paper has not been peer reviewed. Electronic copy available at: https://ssrn.com/abstract=3981895

Pilot-Scale synthesis and manufacturing of SPEEK polymer membrane

The SPEEK (Fig. 2a) polymer was obtained by sulfonation of poly(ether ether ketone) (PEEK) using concentrated sulfuric acid (98 wt%) as the sulfonation reagent. One batch of 1 kg PEEK polymer was gradually added to 10 L concentrated sulfuric acid in a 20 L double glass reactor (Fig. 2b). The solution was mechanically stirred and heated in an oil bath by using a circulating heating tank. The PEEK was sulfonated at 40 °C for reaction time of 7 h to yield SPEEK polymer (Fig. 2c) with a degree of sulfonation of 0.663 (determined by ^{1}H NMR, Supplementary information Fig. S1) and an ion exchange capacity (IEC) of 1.86 meq g^{-1}. The synthesized polymer was washed (Fig. 2c) and dried. Routine characterization analyses confirmed the structure of the polymer and high thermal stability (Supplementary information Fig. S2). The dry SPEEK polymer was first dissolved in N, N-dimethylacetamide (DMAc) to form a 25 wt% solution (Fig. 2d). The resulting polymer solution was then filtered and degassed in a vacuum defoaming machine. Large-area membranes were produced by using a continuous roll-to-roll membrane casting equipment installed in a clean room facility (constant temperature of 25 °C, humidity <20%). The polymer solution was cast onto a polyethylene terephthalate (PET) substrate at a speed of 0.2 m min^{-1} and dried at 50 °C by using the roll-to-roll coater (Fig. 2e). The as-prepared SPEEK membranes with a thickness of ~50 μm are shown in Fig. 2f. Owing to the low cost of raw material ($61.5/kg for PEEK polymer), the cost of SPEEK membrane is estimated to be as low as $12.3 m^{-2}, which is significantly lower than that of commercially available Nafion membranes ($500 m^{-2})[29]. Compared with Nafion 212 membrane, our SPEEK membrane has a higher tensile strength (Fig. 2g), indicating that the mechanical properties of SPEEK membrane meet the practical requirements.

We further evaluated the key performance indicators of ion exchange membranes, such as ionic conductivity, swelling, and alkaline stability (Fig. 1g). To confirm the alkaline stability of the membrane, SPEEK was first treated in 5 mol L^{-1} NaOH solution at 60 °C for 41 days. The mechanical properties of the membranes show negligible differences in elongation at break, tensile strength and tensile strength at break (Fig. 2h), indicating the excellent stability of SPEEK in strong alkaline environment. Further chemical analysis obtained from the FTIR spectra, thermogravimetric analysis (TGA) (Supplementary information Fig. S2) and ^{1}H NMR (Supplementary information Fig. S3) confirmed the high chemical stability of SPEEK. Overall, SPEEK membrane shows advantages over Nafion membrane, owing to its good processability, environmental sustainability, and low cost (Fig. 1g).

This preprint research paper has not been peer reviewed. Electronic copy available at: https://ssrn.com/abstract=3981895

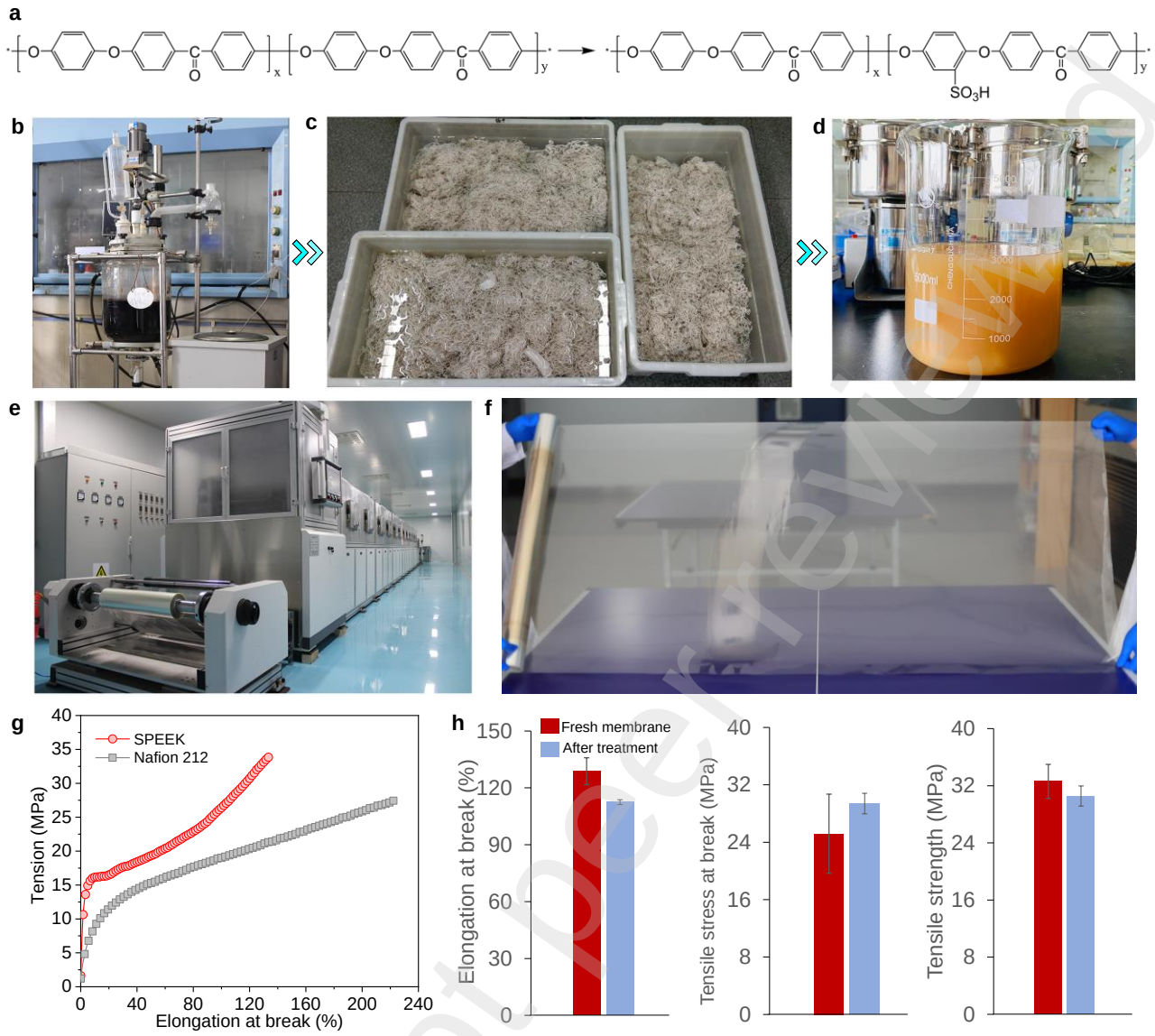


Fig. 2 Pilot scale synthesis and manufacturing of SPEEK membrane. a, The synthesis of SPEEK. **b**, Resin synthesis device with kilogram level and **c**, the synthesized SPEEK polymer. **d**, Photo of the SPEEK polymer solution. **e**, Photo of the roll-to-roll membrane casting machine. **f**, Prepared SPEEK membrane. **g**, Tension-elongation at break curves of SPEEK and Nafion 212 membranes. **h**, The mechanical properties (elongation at break, tensile strength and tensile strength at break) of SPEEK membrane before and after treating the membrane in 5 mol L^{-1} NaOH solution at 60 °C for 41 days.

Electrolyte uptake and ion transport properties

The transport of ions in a membrane depends highly on the supporting electrolyte absorbed in the membrane since the supporting electrolyte acts as the medium to deliver charge carriers. To understand the state and amount of supporting electrolyte in the membrane, we measured the electrolyte uptake and swelling of the SPEEK membrane in different alkaline (KOH and NaOH) electrolytes. The electrolyte uptake and swelling ratio of the SPEEK membrane decrease with increasing alkaline (KOH and NaOH) concentration, respectively (Fig. 3a and 3b). Higher alkaline electrolyte concentration leads to a reduced water activity in the feeding solution and a decreased chemical potential of water exterior to the membrane. Thus, the SPEEK membrane shows a decreased swelling ratio and electrolyte uptake at a higher alkaline concentration.

This preprint research paper has not been peer reviewed. Electronic copy available at: https://ssrn.com/abstract=3981895

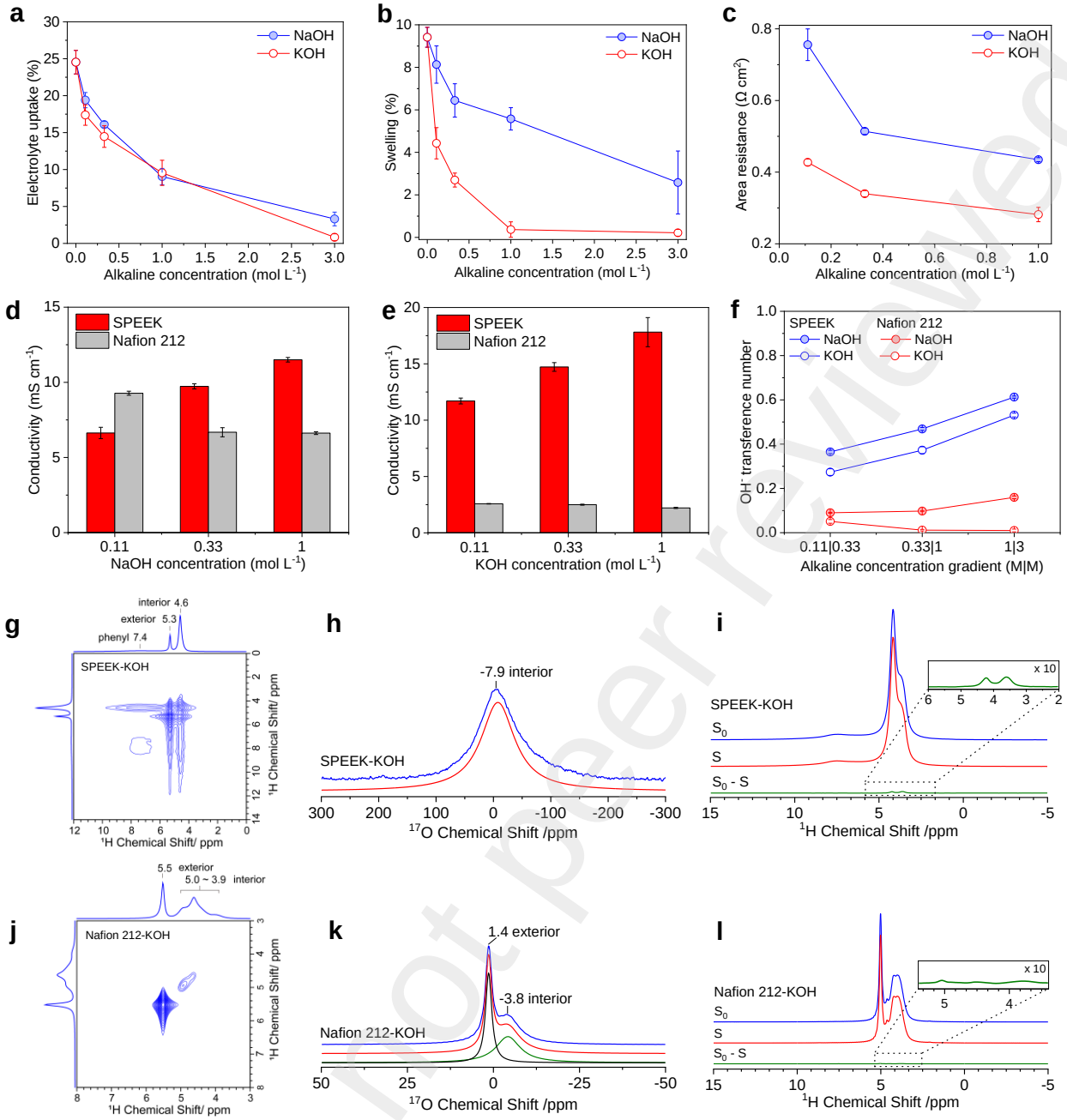


Fig. 3 Properties of the SPEEK membrane in alkaline media. a, Electrolyte uptake, **b**, swelling and **c**, area resistance of SPEEK membrane in alkaline solutions (the original EIS spectra was shown in Supplementary information Fig. S4). Ionic conductivity of SPEEK and Nafion 212 (used as received) membranes in **d**, NaOH and **e**, KOH solutions. **f**, The OH^- transference numbers calculated from V-I profiles for different alkaline concentration gradients in the two reservoirs connected by a SPEEK membrane. Error bars are standard deviations using three measurements from different samples. 2D ^{1}H-^{1}H EXSY NMR spectra for wet samples of **g**, SPEEK-KOH and **j**, Nafion 212-KOH. The deconvolution of the 2D ^{1}H-^{1}H EXSY NMR, and the spectra of both dried samples are presented in Supplementary information Fig. S5. The spectra were acquired using a Bruker AVANCE III HD system with a 9.4 T B_0 field and wide-board 4 mm HXY probe; the spinning frequency was 10 kHz and the mixing time of the 2D EXSY spectra was 0.9 s. SPEEK/Nafion 212 swollen in 3 mol L^{-1} KOH solution: Wet sample: as-prepared membrane with solution on its surface; Dried sample: obtained by air-drying the wet sample for 9 hours at 30% humidity. The ^{17}O spectra of **h**, SPEEK-KOH and **k**, Nafion 212-KOH. The blue lines represent the experimental results, while the red lines represent the overall profile of the deconvolution. The black and green lines represent each signal after deconvolution. The ^{1}H-^{17}O S-RESPDOR experiments of **i**, SPEEK-KOH and **l**, Nafion 212-KOH. The recoupling times of the experiments were 0.4 ms under 10 kHz MAS.

The SPEEK membrane shows a lower areal specific resistance (Fig. 3c) and a higher ionic conductivity (Fig. 3d and 3e) in KOH solution than in NaOH solution at the same concentration. A higher alkaline concentration

This preprint research paper has not been peer reviewed. Electronic copy available at: https://ssrn.com/abstract=3981895

preferentially decreases the membrane areal specific resistance (Fig. 3c) or boosts the membrane ionic conductivity (Fig. 3d and 3e). Compared with Nafion 212 membrane, the SPEEK membrane shows a much higher ionic conductivity (Fig. 3d and 3e). Additionally, the higher alkaline concentration can lead to a lower ionic conductivity in Nafion 212 membrane (Fig. 3d and 3e).

To clarify the ion transport behavior in these membranes, the ion transference number of cations and OH^- through the SPEEK membrane was measured and calculated by evaluating the voltage-current (V-I) profiles (Supplementary information Fig. S6 and S7) in different alkaline concentration gradients (0.11 M|0.33 M, 0.33 M|1 M and 1 M|3 M). Cations (K^+ or Na^+) apparently serve as the dominant charger carriers in the Nafion 212 membrane. In contrast, the OH^- transference number of the SPEEK membrane accounts for a much higher proportion than that of the Nafion 212 membrane (Fig. 3f). When the KOH or NaOH concentration gradient reaches 1 M|3 M (Fig. 3f), the transport of OH^- predominates in KOH or NaOH solution, indicating that the SPEEK membrane preferentially delivers OH^- in a higher alkaline concentration solution.

NMR characterization of ion dynamics

To clarify the transport mechanism of OH^- in the SPEEK membrane, solid-state nuclear magnetic resonance (ssNMR) experiments were further carried out. The ^1H and ^{17}O NMR results demonstrated that the dynamic behaviors of water-related species of SPEEK-KOH and Nafion 212-KOH were significantly different. From ^1H NMR (Supplementary information Fig. S5a) and cross peaks in 2D ^1H-^1H EXSY (Fig. 3g), the single narrow peak ($\delta_{iso}(^1H)$) at 4.6 ppm corresponding to the interior proton species of wet SPEEK-KOH indicated the fast exchange between interior and exterior protons. In comparison, multiple peaks with $\delta_{iso}(^1H)$ values from 5.0~4.0 ppm were observed on the wet Nafion 212-KOH sample (Fig. 3j and Supplementary information Fig. S5b), indicating slow chemical exchange with frequencies less than the $v_{iso}(^1H)$ differences (<400 s^{-1}). The much faster exchange of proton species in SPEEK-KOH revealed by the analysis of spin-spin relaxation time (T_2) (Supplementary information Table S3) enables the fast transport of OH^- in the membrane (Supplementary information Fig. S8), resulting in a high OH^- transference number (Fig. 3f) and high ionic conductivity for SPEEK (Fig. 3d and 3e). The ^{17}O NMR spectra showed opposite mobility of ^{17}O atoms in SPEEK-KOH and Nafion 212-KOH, compared to the ^1H NMR results. The interior ^{17}O (at -7.9 ppm) in SPEEK-KOH exhibited a significantly broader signal (Fig. 3h) than the interior ^{17}O (at -3.8 ppm) in Nafion 212-KOH (Fig. 3k), thus a notably shorter T_2 (Supplementary information Table S4). The broad ^{17}O signal was due to the strongly confined ^{17}O atomic motion which caused large quadrupolar coupling. The narrower interior ^{17}O signal in Nafion-2-KOH indicated significantly less confined motion, comparable to the ^{17}O in exterior water at 1.4 ppm (Fig. 3k). Further, ^1H-^{17}O S-RESPDOR[30] experiments revealed the existence of hydrogen bonding network in SPEEK-KOH, where the dipolar coupling between the strongly confined ^1H and ^{17}O atoms with spatial proximity could cause the loss of

This preprint research paper has not been peer reviewed. Electronic copy available at: https://ssrn.com/abstract=3981895

^{1}H signal intensity (S) compared to the reference spectra (S_0) (Fig. 3i and Supplementary information Fig. S9). In contrast, for Nafion 212-KOH, there was no loss of ^{1}H signal intensity observed (Fig. 3l), thus we speculate that hydrogen bonding network formed in Nafion212 membrane exposed to KOH is much weaker.

To understand the channel structure and distribution of sulfonate groups in membranes, we performed high resolution transmission electron microscopy and small-angle X-ray scattering (SAXS) of Nafion and SPEEK membranes (Supplementary information Fig. S10 and S11-S12). From the TEM imagine, the distribution of -SO_3H groups in SPEEK was random and dispersive, leading to no scattering ionomer peak in the profile. In contrast, the aggregation of –SO_3H groups in Nafion 212 resulted in the formation of ion clusters in the membrane. Although significant research has been done on structure of Nafion membranes and formation of water channels[31], when Nafion membrane is exposed to alkaline solutions, the membrane structure undergoes change due to shrinkage because the alkaline solution narrowed the channels of the Nafion 212 membrane and further decreased the connectivity of the channels. In contrast, the alkaline solution has no significant effect on the ion transport channel of the SPEEK membrane (Supplementary information Fig. S12), which favors the formation of a continuous hydrogen-bonding network among the sulfonated groups, OH^- and free water in the membrane (Fig. 1f).

Combining the results of membrane channel characterization, charge transport properties, and proton exchange experiments, we hypothesize that a portion of the protons inside the SPEEK-KOH membrane traveled quickly, while the oxygen atoms remained relatively stationary, forming hydrogen-bonding networks with a small portion of hydrogen atoms. This hypothesis is in consistent with the Grotthuss mechanism, which can endow the SPEEK membrane with a higher OH^- transference number (Fig. 3f) and high ionic conductivity (Fig. 3d and 3e). In contrast, no obvious dipolar coupling was observed between ^{17}O and ^{1}H atoms (Fig. 3l) or between ^{17}O and backbone ^{19}F atoms in Nafion-212-KOH (Supplementary information Fig. S13). Although the proton exchange in Nafion 212-KOH was slow, the oxygen-containing species (mainly H_2O and OH^-) experienced fast molecular motion. Hence, we propose that the channels in Nafion 212 allow local fast molecular motion of the oxygen-containing species but these species are confined within the poorly connected channels (Fig. 1f), resulting in low conductivity. These new findings challenge the conventional assumptions of ion transport in cation exchange membranes and provide new insights into ion transport membrane and their utilization in alkaline electrolyte-based electrochemical systems.

This preprint research paper has not been peer reviewed. Electronic copy available at: https://ssrn.com/abstract=3981895

Lab-scale single cell performance of alkaline zinc-iron flow battery

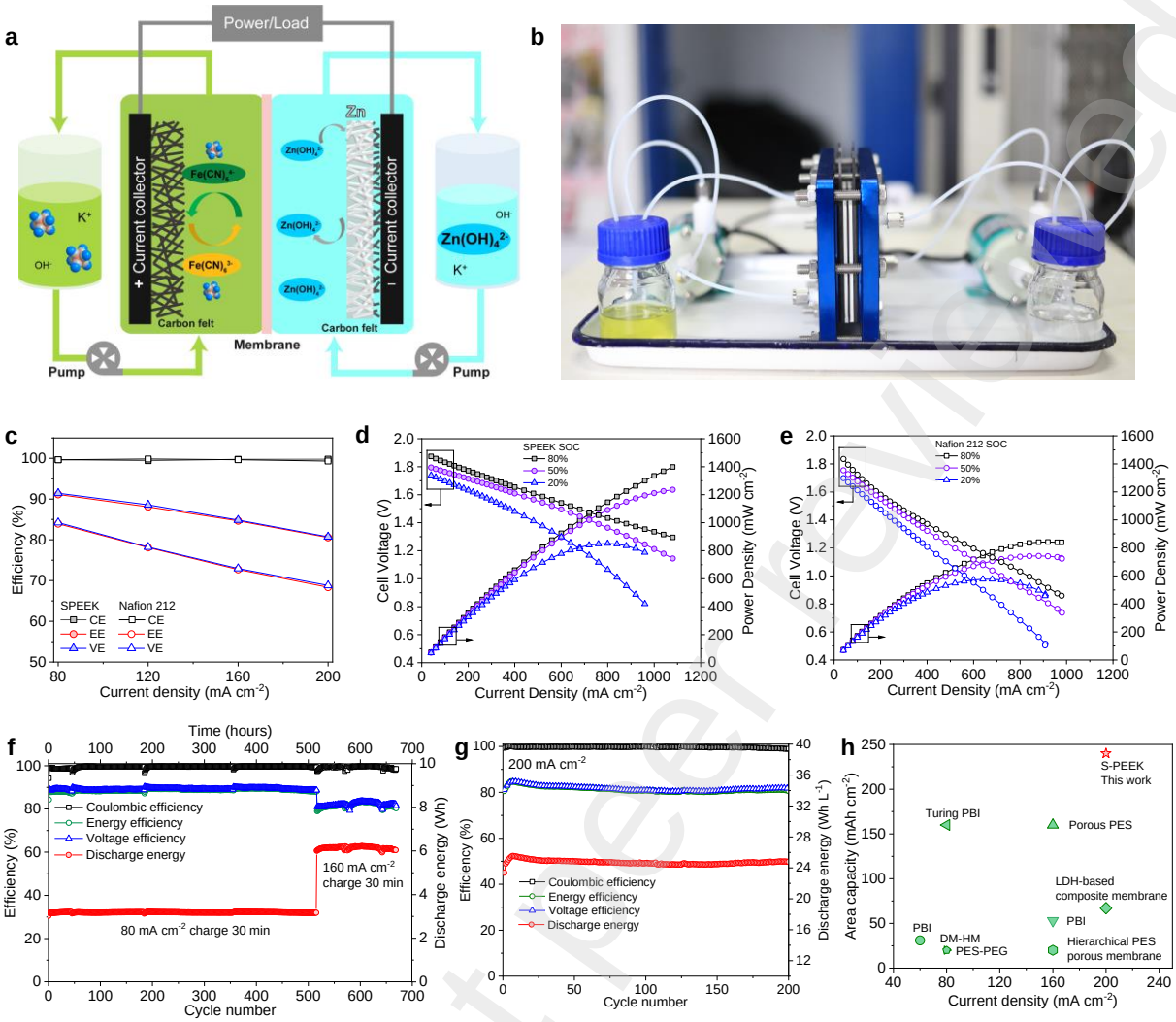


Fig. 4 Performance of the single AZIFB battery. a, Schematic diagram of a single AZIFB. **b**, Photo of a single AZIFB assembled with SPEEK. **c**, Efficiencies of the AZIFB assembled with Nafion 212 and SPEEK at different current densities. 60 mL of 0.8 mol L^{-1} $Na_4Fe(CN)_6$ in 3 mol L^{-1} KOH and 60 mL of 0.4 mol L^{-1} $Na_2Zn(OH)_4$ in 3 mol L^{-1} NaOH were used as positive and negative electrolytes, respectively. The polarization of the AIZFB at different SOC using **d**, SPEEK membrane and **e**, Nafion 212 membrane. The polarization of the AZIFB was measured using a battery with an active area of 9 cm^2. **f**, The alkaline stability of the membrane (cycling performance of AZIFB assembled with the alkaline-treated SPEEK membrane at current densities ranging from 80–160 mA cm^{-2}, inset, discharge energy of the battery). **g**, Cycling performance of the AZIFB assembled with an SPEEK membrane at a current density of 200 mA cm^{-2}. Inset, discharge energy of the battery. Solutions of 60 mL 0.8 mol L^{-1} $Na_4Fe(CN)_6$ in 3 mol L^{-1} KOH and 60 mL 0.4 mol L^{-1} $Na_2Zn(OH)_4$ in 3 mol L^{-1} NaOH were used as positive and negative electrolytes, respectively. **h**, The comparison of performances of recently reported AZIFB. Literature work are included: PBI membrane[10,32]; porous PES membrane[33]; Turing PBI membrane[34]; mixed matrix membrane (DM-HM)[35]; PES-PEG membrane[36]; hierarchical PES porous membrane[37]; LDH-based composite membrane[38].

To demonstrate the application of SPEEK membrane in alkaline battery systems, we assembled an alkaline zinc-iron flow battery with an active membrane area of 48 cm^2 and performed extensive performance testing and control experiments with Nafion membrane (Fig. 4a and 4b). Crossover experiments confirmed the high selectivity of SPEEK membrane towards $Fe(CN)_6^{3-}$ and $Fe(CN)_6^{4-}$ ions (Supplementary information Fig. S14). Owing to the high ionic conductivity of SPEEK membrane in alkaline electrolyte, the flow battery delivered superior performance (Fig. 4c). In particular, the flow battery using the SPEEK membrane provides a coulombic efficiency of 99.5% and a voltage efficiency of 89.8% at a current density of 80 mA cm^{-2} (Supplementary

This preprint research paper has not been peer reviewed. Electronic copy available at: https://ssrn.com/abstract=3981895

information Fig. S15), which is ~9% higher than that assembled from a Nafion 212 membrane (80.9%). A permeation experiment of $Fe(CN)_6^{3-}$/$Fe(CN)_6^{4-}$ through the Nafion 212 and SPEEK membranes was performed to confirm the high selectivity of the membrane. Both Nafion 212 and SPEEK membranes shows a very high selectivity for $Fe(CN)_6^{3-}$/$Fe(CN)_6^{4-}$ (Supplementary information Fig. S14), which contributes to the high coulombic efficiency of the battery. Even at high current density of 200 mA cm^{-2}, the battery still provides high coulombic efficiency of 99.78% and an energy efficiency of 80.57% (Fig. 4c). The battery assembled with SPEEK membrane delivers a much higher efficiency than that using a Nafion 212 membrane. Combining the high open cell voltage (OCV, Supplementary information Fig. S16) of the battery and the high ion conductivity of SPEEK membrane, the flow battery can provide a superior power density (Fig. 4d), which is much higher than that of Nafion 212 membrane (Fig. 4e).

In zinc-based batteries, zinc dendrite associated with zinc anodes usually leads to battery failure and poor cycle life, especially at a high working current density[33]. In a cation-exchange membrane system, negatively charged cationic groups (sulfonic acid groups) can impart the membrane with a negative electrostatic potential (ESP) distribution (Fig. 1e and Supplementary information Fig. S17), which favors the plating-stripping process of the zinc couple on the electrode[33] and further enables a high-rate-performance alkaline zinc-iron flow battery with a long cycle life. Using this advantage, a 4-hour plating process performed at 40 mA cm^{-2} and a nearly 2-hour stripping process performed at 80 mA cm^{-2} were realized (Supplementary information Fig. S18), yielding a high areal discharge capacity of 158 mAh cm^{-2} (Supplementary information Fig. S18). By altering the operational mode of the battery (8 hours of plating at 20 mA cm^{-2} and stripping at 160 mA cm^{-2} and 80 mA cm^{-2}, respectively) (Supplementary information Fig. S19), a discharge capacity of ~7.60 Ah and a discharge energy of ~12.90 Wh for the AZIFB remained, demonstrating the operational flexibility of the battery.

To further study the stability of the membrane, we treated the SPEEK membrane by 5 mol L^{-1} NaOH solution at 60 °C for 41 days and then assembled the flow battery and carried out long term cycling. The battery showed stable cycling performance for more than 650 cycles (more than 650 hours) at current densities ranging from 80 mA cm^{-2} to 160 mA cm^{-2} (Fig. 4f), indicating that this hydrocarbon-based cation-exchange membrane demonstrates prominent stability in alkaline media. Even operating at a current density as high as 200 mA cm^{-2}, the flow battery can still provide a stable performance for more than 200 cycles and maintain a stable discharge energy (Fig. 4g), which demonstrated high stability of SPEEK membrane. Overall, the SPEEK membrane demonstrated the best performances among recently reported membranes utilized in AZIFB (Fig. 4h) owing to their high ionic conductivity and chemical stability.

Lab-scale single cell performance of alkaline organic flow battery

To further demonstrate the broad application of SPEEK membrane in alkaline media, we also assembled the

This preprint research paper has not been peer reviewed. Electronic copy available at: https://ssrn.com/abstract=3981895

membrane in an alkaline quinone-iron flow battery and measured the single cell performance (Fig. 1b and Supplementary information Fig. S20). Owing to the high ionic conductivity, an alkaline quinone-iron flow battery using the SPEEK membrane demonstrated a voltage efficiency of 90.8% and an energy efficiency of 89.0% at 40 mA cm^{-2}, which is higher than that of a Nafion 212 membrane (energy efficiency of 85.8%) at the same condition. Even at a current density of 80 mA cm^{-2}, the battery shows high coulombic efficiency of 98.9% and an energy efficiency of 81.9%, together with a stable performance for more than 100 cycles. The battery capacity decay was mainly due to the degradation of quinone molecules during cycling of the alkaline electrolytes instead of the membrane degradation or crossover.[4]

Commercial kW-scale flow battery stack performance

One unique feature of flow battery is the upscaling of decoupled power and energy. Scaling up the membrane area in the flow battery stack provides high output power (Fig. 5a), while the energy or capacity can be scaled up by increasing the volume of the electrolytes. To further demonstrate the performance of the SPEEK membrane, we scaled up the flow battery cell stacks ranging from 300 W to 4000 W with membrane areas scaled up from 4375 cm^2 to 3 m^2 and the energy efficiency of the stack remained nearly unchanged (Fig. 5b). Such upscaling of flow battery stack is crucial to solve the bottleneck of commercialization of flow battery technology.

Firstly, a 300 W flow battery stack comprising 5 single cells (with an active area 875 cm^2 for each single cell) was assembled (Fig. 5c). The voltage of the stack ranges from 8 V-9.5 V at a constant current (35 A) (Fig. 5d). The stack could run stably for more than 400 cycles (more than 800 hours) at a current density of 40 mA cm^{-2} (Fig. 5i, areal capacity of 40 mAh cm^{-2}), together with an average coulombic efficiency of 98.2%, an average energy efficiency of 87.8% and an average output power of 291 W (Fig. 5i). Furthermore, we increased the size (1000 cm^2) and number of cell stacks (10 single cells, Fig. 5e) to yield a 1000 W cell stack, delivering an average discharge voltage of 16.67 V at a current of 80 A (1333 W, Fig. 5f). By using SPEEK membrane, the stack showed an average coulombic efficiency of 98.4% and an average energy efficiency of 85.03% for more than 200 cycles operated at 80 mA cm^{-2} (Supplementary information Fig. S21, areal capacity of 80 mAh cm^{-2}). A stable discharge capacity and discharge energy could be maintained for more than 200 cycles (Supplementary information Fig. S21), giving a total discharge energy of 265.11 kWh. The voltage (current)-time curves (18^{th}, 152^{nd}) in Fig. 5e further confirm the stability of the cell stack using the SPEEK membrane. A 4000 W cell stack was constructed by further increasing the number of single cells from 10 to 15 and the active area of each cell from 1000 cm^2 to 2000 cm^2, (Fig. 5g). The stack showed an average coulombic efficiency of 97.8% and an average energy efficiency of 85.5% at 80 mA cm^{-2} (Supplementary information Fig. S22), along with a discharge capacity of ~117 Ah and a discharge energy of ~2.91 kWh for each cycle (Supplementary information Fig. S22). At a current density of 80 mA cm^{-2} (160 A, Fig. 5h), the stack exhibited an average discharge voltage of 24.95 V (Fig. 5h),

This preprint research paper has not been peer reviewed. Electronic copy available at: https://ssrn.com/abstract=3981895

providing an output power of 3992 W. These results demonstrated the great potential of SPEEK membrane for alkaline-based battery systems.

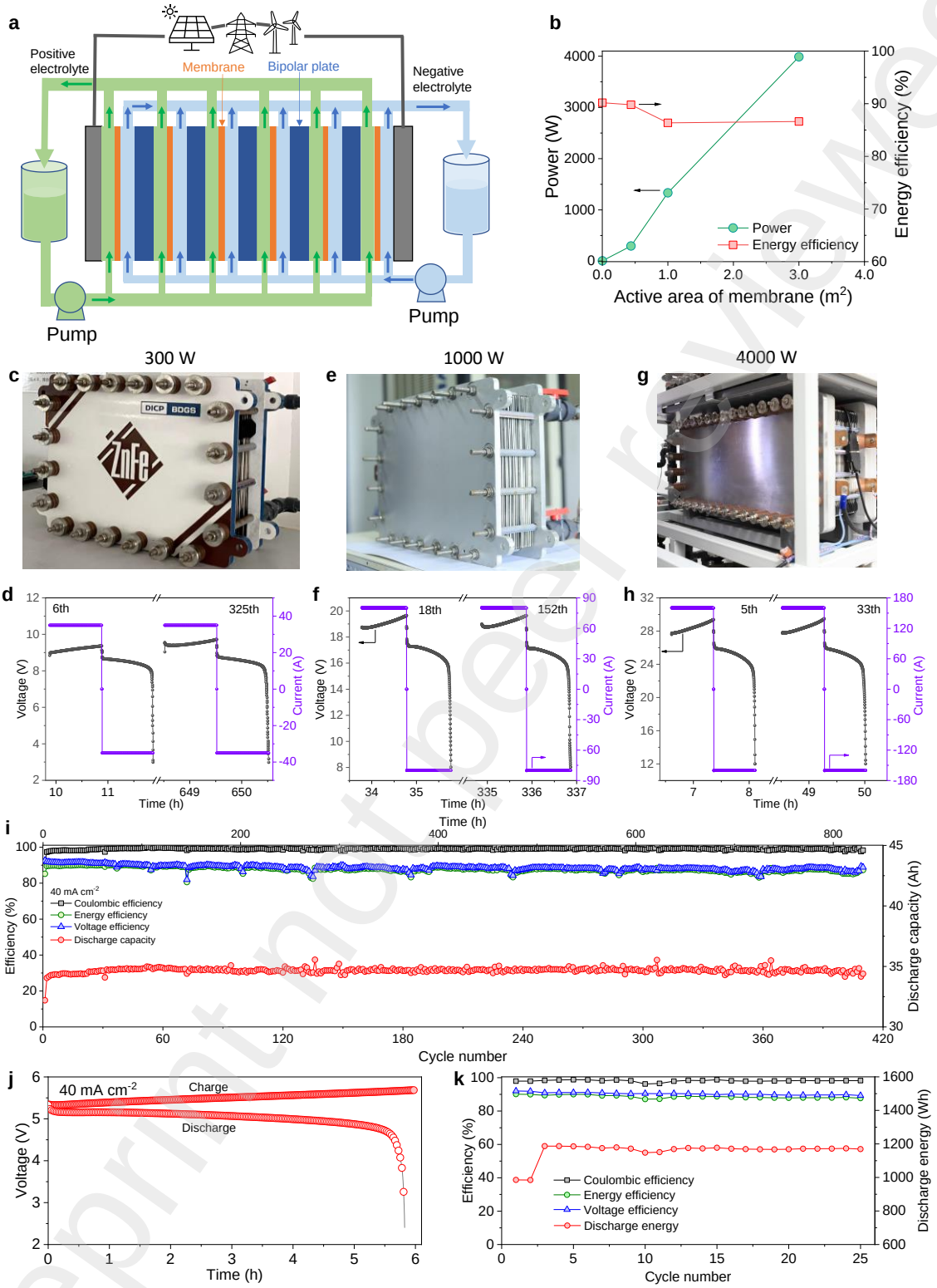


Fig. 5 Performances of AZIFB cell stacks assembled with the SPEEK membrane. a, The schematic diagram of the cell stack. **b**, Effect of membrane area on power and energy efficiency of flow battery stack. **c**, Photo of 300 W flow battery stack. **d**, The voltage (current)-time curves (6^{th}, 325^{th}) operated at 40 mA cm^{-2}. **e**, Photo of 1000 W stack. **f**, The voltage (current)-time curves (18^{th}, 152^{nd}) operated at 80 mA cm^{-2}. **g**, Photo of 4000 W stack. **h**, The voltage (current)-time curves (5^{th}, 33^{rd}) operated at 80 mA cm^{-2}. **i**, The cycling performance of flow battery stack comprising 5 single cells using the SPEEK membrane operated at 40 mA cm^{-2}. **j**, The charge-discharge curve of flow battery stack (3 single cells with active area of each cell at 1000 cm^2, ~12 hours charging-discharging for each cycle, 40 mA cm^{-2}) in long-duration energy storage experiment. **k**, The long-duration energy storage performance of the alkaline zinc-iron flow battery stack.

This preprint research paper has not been peer reviewed. Electronic copy available at: https://ssrn.com/abstract=3981895

The long-duration energy storage has been identified as a promising solution to address intermittency in renewable energy supply[1]. To evaluate the long-duration and long-term energy storage performance of AZIFB, a stack consisting of 3 single cells (with an active area of 1000 cm^2 for each single cell) was assembled and tested with long duration charging for 6 h and a 6 h discharging at 40 mA cm^{-2} (Fig. 5j). A high battery efficiency up to 88% was achieved (Fig. 5k) and the stack delivered an areal charge capacity of 240 mAh cm^{-2} and a discharge energy of ~1.17 kWh for each cycle (Fig. 5k), showing great potential for long-duration energy storage.

Cost analysis

One critical bottleneck for upscaling of flow battery for grid scale long duration storage is the cost of flow battery stack, particularly the membranes and electrolytes[1,39]. One key strategy to reduce the cost of battery is to replace the expensive Nafion membrane with low cost hydrocarbon membranes, as well as development of low cost electrolytes. The cost of electrolytes ($Fe(CN)_6^{4-}/Fe(CN)_6^{3-}$, $Zn(OH)_4^{2-}$) for alkaline zinc-iron flow battery can reach as low as ~$40/kWh, which is much lower than that of vanadium flow battery. Low-cost hydrocarbon membrane could further reduce the cost of the alkaline zinc-iron flow battery.

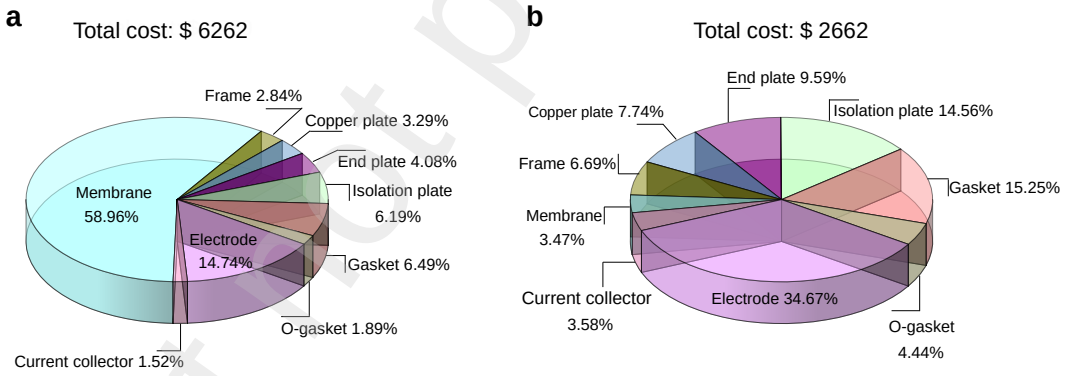


Fig. 6 Cost analysis based on a 10 kW stack. a, The cost analysis of a 10 kW cell stack based on **a**, Nafion 212 membrane. **b**, The cost analysis of a 10 kW cell stack based on a SPEEK membrane.

Figure 6 shows the comparison of costs of a 10-kW alkaline zinc-iron cell stack based on a Nafion 212 membrane and SPEEK membrane. The detailed cost and the amount of components for the 10-kW cell stack were provided in Supplementary information Table 5. The Nafion membrane cost accounted for the highest proportion (~59%), followed by the electrode cost. By contrast, by replacing the Nafion 212 membrane with the SPEEK membrane, the cost of the 10-kW cell stack dramatically decreased to $2662, with the membrane cost accounted for the lowest proportion (3.47%), indicating that reducing the membrane cost can significantly reduce the capital cost of flow battery in practical application. Based on this analysis, a 100 MW-scale energy storage plants will require at least 75,000 m^2 ion exchange membranes (Supplementary information Fig. S23). The cost of the membrane

This preprint research paper has not been peer reviewed. Electronic copy available at: https://ssrn.com/abstract=3981895

would dramatically decrease from $277 million (Nafion 212) to $6.9 million (SPEEK) (Supplementary information Fig. S23). According to the Renewables 2020 Analysis and forecast to 2025 (November 2020 by International Energy Agency), net installed renewable capacity has grown by nearly 4% globally in 2020, reaching almost 200 GW, and total installed power capacity by solar and wind in 2025 will reach 2,349 GW. Even if only 10% renewable energy is stored, that is equivalent of more than 234 GW energy storage capacity. Thus, reducing the energy storage capital cost is of the greatest importance. Replacing the high-cost Nafion membrane with the cost-effective SPEEK membrane significantly reduces the energy storage capital cost, which is highly beneficial to accelerate the large-scale deployment of renewable energy infrastructure.

Conclusion

In summary, we have demonstrated the upscaling of next-generation alkaline-based flow batteries using a low-cost hydrocarbon ion exchange membrane with excellent alkaline stability and achieved superior performance from lab-scale to kW scale stacks. The SPEEK membrane showed good mechanical property, high chemical stability in alkaline media, and reasonably high ionic conductivity. NMR experiments revealed that the transport of OH^- in the SPEEK membrane followed Grotthuss mechanisms. These scientific findings challenge the conventional knowledge in ion transport in cation exchange membranes, and provide a new perspective on membrane design and their utilization in alkaline electrolyte-based electrochemical systems. The SPEEK membrane shows superior performance in an alkaline zinc-iron flow battery, as tested in single cells and cell stacks ranging from 300 W to 4000 W, showing a high energy efficiency of 85.46% for a 4000 W stack operated at 80 mA cm^{-2}, and long term stability over 800 h. Cost analysis confirmed a significant capital cost reduction of flow battery stack which will advance the manufacturing of flow battery system for large scale energy storage plants. Our work bridged the gap between laboratory scale battery component development and industrial scale flow battery stack operation. We expect that our work will inspire the development of next-generation cost-effective flow batteries based on low-cost hydrocarbon membranes for large scale long-duration energy storage applications.

References

1 Sepulveda, N. A., Jenkins, J. D., Edington, A., Mallapragada, D. S. & Lester, R. K. The design space for long-duration energy storage in decarbonized power systems. *Nature Energy* **6**, 506-516, (2021).

2 Dunn, B., Kamath, H. & Tarascon, J.-M. Electrical energy storage for the grid: a battery of choices. *Science* **334**, 928-935 (2011).

3 Jiao, K. *et al.* Designing the next generation of proton-exchange membrane fuel cells. *Nature* **595**, 361-369 (2021).

4 Zhao, E. W. *et al.* In situ NMR metrology reveals reaction mechanisms in redox flow batteries. *Nature* **579**, 224-228 (2020).

5 Hu, B. & Liu, T. L. Tanking up energy through atypical charging. *Science* **372**, 788-789, (2021).

6 Park, M., Ryu, J., Wang, W. & Cho, J. Material design and engineering of next-generation flow-battery

This preprint research paper has not been peer reviewed. Electronic copy available at: https://ssrn.com/abstract=3981895

technologies. *Nature Reviews Materials* **2**, 16080, (2016).
7 Arora, P. & Zhang, Z. Battery Separators. *Chemical Reviews* **104**, 4419-4462, (2004).
8 Mauritz, K. A. & Moore, R. B. State of Understanding of Nafion. *Chemical Reviews* **104**, 4535-4586, (2004).
9 Yuan, Z. *et al.* Advanced Materials for Zinc-Based Flow Battery: Development and Challenge. *Advanced Materials* **31**, 1902025, (2019).
10 Yuan, Z., Duan, Y., Liu, T., Zhang, H. & Li, X. Toward a low cost alkaline zinc-iron flow battery with a polybenzimidazole custom membrane for stationary energy storage. *iScience*, **3**, 40-49 (2018).
11 Huskinson, B. *et al.* A metal-free organic-inorganic aqueous flow battery. *Nature* **505**, 195-198, (2014).
12 Lin, K. *et al.* Alkaline quinone flow battery. *Science* **349**, 1529-1532, (2015).
13 Wang, Y.-J., Qiao, J., Baker, R. & Zhang, J. Alkaline polymer electrolyte membranes for fuel cell applications. *Chemical Society Reviews* **42**, 5768-5787, (2013).
14 Steele, B. C. H. & Heinzel, A. Materials For Fuel-Cell Technologies. *Nature* **414**, 345-352 (2001).
15 Viswanathan, V. *et al.* Cost and performance model for redox flow batteries. *Journal of Power Sources* **247**, 1040-1051, (2014).
16 Zhang, M., Moore, M., Watson, J. S., Zawodzinski, T. A. & Counce, R. M. Capital Cost Sensitivity Analysis of an All-Vanadium Redox-Flow Battery. *Journal of The Electrochemical Society* **159**, A1183-A1188, (2012).
17 Grey, C. P. & Tarascon, J. M. Sustainability and in situ monitoring in battery development. *Nature Materials* **16**, 45, (2016).
18 Darling, R. M., Gallagher, K. G., Kowalski, J. A., Ha, S. & Brushett, F. R. Pathways to low-cost electrochemical energy storage: a comparison of aqueous and nonaqueous flow batteries. *Energy & Environmental Science* **7**, 3459-3477, (2014).
19 Shin, D. W., Guiver, M. D. & Lee, Y. M. Hydrocarbon-Based Polymer Electrolyte Membranes: Importance of Morphology on Ion Transport and Membrane Stability. *Chemical Reviews* **117**, 4759-4805, (2017).
20 Merle, G., Wessling, M. & Nijmeijer, K. Anion exchange membranes for alkaline fuel cells: A review. *Journal of Membrane Science* **377**, 1-35, (2011).
21 Pan, J. *et al.* A strategy for disentangling the conductivity–stability dilemma in alkaline polymer electrolytes. *Energy & Environmental Science* **6**, 2912-2915, (2013).
22 De Porcellinis, D. *et al.* Communication—Sulfonated Poly (ether ether ketone) as Cation Exchange Membrane for Alkaline Redox Flow Batteries. *Journal of The Electrochemical Society* **165**, A1137-A1139, (2018).
23 Couture, G., Alaaeddine, A., Boschet, F. & Ameduri, B. Polymeric materials as anion-exchange membranes for alkaline fuel cells. *Progress in Polymer Science* **36**, 1521-1557 (2011).
24 Arges, C. G. & Ramani, V. Two-dimensional NMR spectroscopy reveals cation-triggered backbone degradation in polysulfone-based anion exchange membranes. *Proceedings of the National Academy of Sciences* **110**, 2490-2495 (2013).
25 Varcoe, J. R. *et al.* Anion-exchange membranes in electrochemical energy systems. *Energy & Environmental Science* **7**, 3135-3191, (2014).
26 Yuan, Z., Zhang, H. & Li, X. Ion conducting membranes for aqueous flow battery systems. *Chemical Communications* **54**, 7570 (2018).
27 Tan, R. *et al.* Hydrophilic microporous membranes for selective ion separation and flow-battery energy storage. *Nature Materials* **19**, 195-202, (2020).
28 Baran, M. J. *et al.* Design Rules for Membranes from Polymers of Intrinsic Microporosity for Crossover-free Aqueous Electrochemical Devices. *Joule* **3**, 2968-2985, (2019).
29 Tsehaye, M. T., Alloin, F. & Iojoiu, C. Prospects for Anion-Exchange Membranes in Alkali Metal–Air Batteries. *Energies* **12**, 4702 (2019).

This preprint research paper has not been peer reviewed. Electronic copy available at: https://ssrn.com/abstract=3981895

30 Chen, L. *et al.* Measurement of hetero-nuclear distances using a symmetry-based pulse sequence in solid-state NMR. *Physical Chemistry Chemical Physics* **12**, 9395-9405, (2010).
31 Schmidt-Rohr, K. & Chen, Q. Parallel cylindrical water nanochannels in Nafion fuel-cell membranes. *Nature Materials* **7**, 75, (2007).
32 Chen, Z. *et al.* Mathematical modeling and numerical analysis of alkaline zinc-iron flow batteries for energy storage applications. *Chemical Engineering Journal* **405**, 126684, (2021).
33 Yuan, Z. *et al.* Negatively charged nanoporous membrane for a dendrite-free alkaline zinc-based flow battery with long cycle life. *Nature Communications* **9**, 3731, (2018).
34 Wu, J. *et al.* Dendrite-Free Zinc-Based Battery with High Areal Capacity via the Region-Induced Deposition Effect of Turing Membrane. *Journal of the American Chemical Society* **143**, 13135-13144, (2021).
35 Chang, N. *et al.* A Cost-Effective Mixed Matrix Polyethylene Porous Membrane for Long-Cycle High Power Density Alkaline Zinc-Based Flow Batteries. *Advanced Functional Materials* **29**, 1901674, (2019).
36 Chen, D., Kang, C., Duan, W., Yuan, Z. & Li, X. A non-ionic membrane with high performance for alkaline zinc-iron flow battery. *Journal of Membrane Science* **618**, 118585, (2021).
37 Hu, J. *et al.* A highly stable membrane with hierarchical structure for wide pH range flow batteries. *Journal of Energy Chemistry* **56**, 80-86, (2021).
38 Hu, J. *et al.* Layered double hydroxide membrane with high hydroxide conductivity and ion selectivity for energy storage device. *Nature Communications* **12**, 3409, (2021).
39 Noack, J., Wietschel, L., Roznyatovskaya, N., Pinkwart, K. & Tübke, J. Techno-Economic Modeling and Analysis of Redox Flow Battery Systems. *Energies* **9**, 627 (2016).

Preprint not peer reviewed

This preprint research paper has not been peer reviewed. Electronic copy available at: https://ssrn.com/abstract=3981895

Methods

Materials. Poly(ether ether ketone) (PEEK) was kindly provided by Changchun Jilin University Special Plastic Engineering Research. N,N-dimethylacetamide (DMAc) were purchased from Tianjin Damao Chemical Reagent Factory. Sodium ferrocyanide was bought from Sinopharm Chemical Regent Co.,Ltd. Zinc oxide was bought from Kermel Chemical Reagent Factory. These reagents were supplied with analytical grade. Alizarin red (ARS), sodium hydroxide (99.9% metals basis) and potassium hydroxide (electronic grade) were brought from Aladdin, Shanghai, and used as received. Other reagents were brought from Sigma Aldrich unless stated otherwise and used as received. Nafion 212 membrane was obtained from Dalian Northern Key Import & Export Co., LTD and used as received.

Synthesis of SPEEK polymers. The SPEEK polymer was prepared by direct sulfonation of poly(ether ether ketone) (PEEK) using concentrated sulfuric acid (98 wt%) as the sulfonation reagent. 1 kg of PEEK powder was added to 10 L concentrated sulfuric acid in a 20 L double glass reactor. The solution was mechanically stirred. The sulfonated reaction was carried out at 40 °C for 7 h to synthesize SPEEK polymer. The degree of sulfonation (DS) was determined by ^{1}H NMR and calculated as follows[40]:

$$\frac{DS}{12-2DS} = \frac{A_{H_1}}{\sum A_{H_N}}$$

Where A_{H_1} represents the integration area of H peak (ortho-position of –SO_3H), $\sum A_{H_N}$ indicates the integration area of all proton peaks.

The IEC of SPEEK can calculate from DS value as follows[41]:

$$\mathrm{DS} = \frac{288 \times IEC}{1000 - 102 \times IEC}$$

Manufacturing of membranes. The dry SPEEK polymer was first dissolved in N, N-dimethylacetamide (DMAc) to form a 25 wt% solution and then filtered and defoamed in a vacuum defoaming machine. Large-area membranes were produced by using a continuous roll-to-roll membrane casting equipment. The polymer solution was cast onto a polyethylene terephthalate (PET) substrate at a speed of 0.2 m min^{-1} and dried at 50 °C by using an automatic coater, which was completed in a clean room facility with a constant temperature of 25 °C and a humidity less than 20%. Afterwards, the membrane was peeled off and the thickness of the membrane was ~50 μm.

Characterization of polymers and membranes.

FTIR. Attenuated total reflection Fourier transform infrared spectroscopy (FTIR, Nicolet iS50, Thermo Fisher Co., Ltd.), recorded at a rate of 48 scans with a resolution of 4 cm^{-1} and collected from 500 to 4000 cm^{-1} in reflection mode, was carried out to confirm the structure and alkaline stability of the SPEEK membrane.

Thermogravimetric analysis (TGA). TGA experiments were carried out to investigate the thermal stability of SPEEK membrane before and after alkaline treatment. The experiments were performed on a PerkinElmer Pyris Diamond TG/DTA instrument with a heating rate of 10 °C min^{-1} at an argon atmosphere. Before measurement, the sample was hold at 80 °C for 30 mins to remove free water in the membrane.

Small angle X-ray scattering (SAXS). SAXS patterns of the dry SPEEK, dry Nafion 212, water treated SPEEK and Nafion 212, 0.5 mol L^{-1} NaOH treated SPEEK and Nafion 212 and 0.5 mol L^{-1} KOH treated SPEEK and Nafion 212 were performed on a Rigaku Smart Lab between 0.6° and 5°. The scattering vector was calculated according to following equation:

$$\mathrm{q} = \frac{2\pi \sin\theta}{\lambda}$$

Where 2θ is the scattering angle and λ is the scattering wave length, 0.1541 nm.

The Bragg spacing was calculated as follows: $\mathrm{d} = {}^{2\pi}/_{q}$

Distribution of –SO_3H in SPEEK and Nafion 212 membranes. The distribution of –SO_3H in SPEEK membrane was recorded by using a transmission electron microscope (TEM) (JEM-2000EX, JEOL). The SPEEK membrane was first treated in a silver nitrate (0.1 mol L^{-1}) for 6 days and then washed with ultrapure water. The resulted SPEEK was fixed in epoxy, before cutting into thin slice samples. As a reference, the distribution of –SO_3H in a Nafion 212 was also investigated. Nafion 212 was first converted to the Pb^{2+} form by soaking in a lead acetate solution (0.5 mol

This preprint research paper has not been peer reviewed. Electronic copy available at: https://ssrn.com/abstract=3981895

L^{-1}) for 3 days and then washed with ultrapure water. The obtained Nafion 212 was fixed in epoxy, before cutting them into thin slices. The samples were cast onto a Cu grid for TEM study.

Density functional theory (DFT) calculations. To study the electrostatic potential of the membranes, DFT calculation was carried out using Gaussian 16 package[42]. The structures were firstly optimized at M06-2X[43] hybrid functional with def2-SVP[44] basis set including the atom-pairwise dispersion correction (DFT-D3)[45,46]. Then a single point energy calculation was performed at M06-2X/def2-TZVP level to obtain the wave function of each optimized structure. The electrostatic potential surface (ESP) were analyzed by Multiwfn[47] package on an isosurface of electronic density at 0.001 a.u. and drawn by VMD[48] package.

NMR experiments. The NMR experiments for ion transport behavior in the membranes were conducted on Bruker AVANCE III HD wide-bore spectrometer with 9.4 T B_0 field. The ^{1}H spectra of SPEEK-KOH and Nafion-212-KOH were acquired by spin-echo experiments, with 90° pulse length being 7.7 and 6.1 μs. The ^{1}H-^{1}H NOESY used the same 90° pulse and 0.9 s mixing time. Both the 1D ^{1}H spectra and 2D ^{1}H-^{1}H NOESY were conducted at 4 mm HXY triple-resonance probe at 10 kHz MAS condition. The ^{17}O spectra was acquired by one-pulse experiments with 4.8 μs pulse length (52 kHz) at 12 kHz MAS. In S-RESPDOR[49] experiments, the dipolar couplings were reintroduced by SR4 sequence with radiofrequency amplitude of 20 kHz, and the recoupling time was 0.4 ms. In the ^{17}O isotropic labeling, 0.0257 g SPEEK-KOH and 0.0276 g Nafion-212-KOH were first dried in 30% humidity for 9 h to reduce the exterior water and then 3 μL of $^{17}OH_2$ was added for ^{17}O exchange. In ^{1}H-^{17}O S-RESPDOR for SPEEK-KOH and Nafion-212-KOH, the 90° pulse for ^{1}H excitation were 4.6 and 3.7 μs, while for ^{19}F-^{17}O S-RESPDOR experiments, the 90° pulse for ^{19}F excitation was 3.7 μs. All the Mas condition of S-RESPDOR experiments was 10 kHz.

The permeability of OH^- through the membranes.

The permeability of OH^- across the membranes was measured using an osmosis cell, and the concentration of OH^- was measured by Mettler Toledo pH meter. The feeding solution and the diffusion side were using 3 mol L^{-1} OH^- and ulta-pure water, respectively.

Swelling and electrolyte uptake of the membranes.

The swelling and electrolyte uptake of the membrane under different conditions were measured by comparing the area and weight change before and after immersing the membranes in different solutions (water, 0.11 mol L^{-1} NaOH, 0.33 mol L^{-1} NaOH, 1 mol L^{-1} NaOH, 3 mol L^{-1} NaOH, 0.11 mol L^{-1} KOH, 0.33 mol L^{-1} KOH, 1 mol L^{-1} KOH, 3 mol L^{-1} KOH) for 72 h at room temperature. The membrane sample with fixed size and weight was dried at 50 °C for 24 h prior to soaking in the above solutions. The swelling and electrolyte uptake of SK-2 was calculated by the following equations:

$$\text{Swelling}(\%) = \frac{A_w - A_d}{A_d} \times 100$$

$$\text{Electrolyte uptake}(\%) = \frac{m_w - m_d}{m_d} \times 100$$

where A_w *and* A_d are the areas of wet and dry membrane, respectively, m_w *and* m_d are the weights of wet and dry membrane, respectively.

Area resistance and ionic conductivity.

The area resistance of the prepared membranes under different solutions (0.11 mol L^{-1} NaOH, 0.33 mol L^{-1} NaOH, 1 mol L^{-1} NaOH; 0.11 mol L^{-1} KOH, 0.33 mol L^{-1} KOH, 1 mol L^{-1} KOH) was tested by the electrochemical impedance spectroscopy (EIS) testing station (Solartron SI 1260 and SI 1287) according to the method as reported[50]. Five pieces of membranes were stacked together and sandwiched between two round titanium plates. The effective diameter for each pieces of membrane was 1.5 cm. 1 to 5 pieces of membranes were stacked together and the corresponding resistances were measured (Supplementary Figure 4). The area resistance for one pieces of membrane (R) was calculated by plotting the total resistances to the number of membranes stacked. Each result was an average value of three parallel experiments. The frequency of EIS was set from 1000 Hz to 1000 kHz. The membranes were pretreated in corresponding alkaline solutions for 24 h.

The ionic conductivity of the membranes in different solutions was calculated by the following equation: σ=L/R.

This preprint research paper has not been peer reviewed. Electronic copy available at: https://ssrn.com/abstract=3981895

Where σ (S cm^{-1}) is the ionic conductivity of the membrane, L (cm) is the thickness of the membrane, R (Ω cm^2) is the area resistance of the membrane. Each result was an average value of three parallel experiments.

Ion transference numbers.

The ion transport numbers for the cation-exchange membranes (SPEEK and Nafion 212) were investigated using Gamry Multichannel System installation (Reference 3000). The voltage-current (V-I) profile was recorded when the membrane was sandwiched between two cells soaking with different alkaline (NaOH and KOH) concentration gradients (0.11 M|0.33 M, 0.33 M|1 M and 1 M|3 M, respectively). Two Ag/AgCl reference electrodes filled in saturated KCl solution and two salt bridges filled in saturated KCl solution were employed to eliminate the potential drop caused by the unequal potential drop at the electrode-solution interface[51,52] and the liquid junction potential generated by two different electrolytes. Thus the open-cell voltage of the device (V_0) is equal to the value of diffusion potential (V_d) resulted from the alkaline concentration gradient, which can be calculated as the following equation:

$$V_O = V_d = \frac{RT}{F}(t_{K^+ \text{ or } Na^+} - t_{OH^-})\ln(\Delta)$$

R, T, F, $t_{K^+ \text{ or } Na^+}$, t_{OH^-} *and* Δ are the gas constant, temperature, faraday constant, K^+ or Na^+ transference number, OH^- transference number and concentration gradient, respectively. Of note is that if the alkaline concentration gradient is high (e.g., 1 M|3 M), the mean activity coefficient of ions for the alkaline solution (Δ) must be considered.

Permeability of $Fe(CN)_6^{4-}$/$Fe(CN)_6^{3-}$ through the membranes.

The permeability of $Fe(CN)_6^{4-}$/$Fe(CN)_6^{3-}$ through the membrane was determined by a diffusion cell separated by a membrane. The left cell was filled with 0.4 mol L^{-1} $Fe(CN)_6^{4-}$/$Fe(CN)_6^{3-}$ in 3 mol L^{-1} alkaline solution (volume: 80 mL) while the right one was filled with 3 mol L^{-1} alkaline solution (volume: 80 mL). Solutions in both half cells were vigorously stirred to avoid concentration polarization. The effective area of the membrane was 9 cm^2. Samples of a 3 mL solution from the right cell were collected at a regular time interval. Another 3 mL fresh alkaline solution was then added to the right cell to keep the solution volume stable. The $Fe(CN)_6^{4-}$ or $Fe(CN)_6^{3-}$ concentration of the samples was detected using a UV-vis spectrometer (TU-1901, Beijing Purkinje General Instrument Co., Ltd.). The permeability of $Fe(CN)_6^{4-}$/$Fe(CN)_6^{3-}$ was calculated according to Fick's diffusion law as the following equation:

$$V_B \frac{dC_B(t)}{dt} = A\frac{P}{L}(C_A - C_B(t))$$

where V_B is the solution volume in the right reservoir, $C_B(t)$ is $Fe(CN)_6^{4-}$ or $Fe(CN)_6^{3-}$ concentration in the left cell as a function of time t (h), while A and L are the effective area (cm^2) and thickness (cm) of the membrane, respectively. P is the permeability of $Fe(CN)_6^{4-}$ or $Fe(CN)_6^{3-}$, and C_A is the concentration of $Fe(CN)_6^{4-}$ or $Fe(CN)_6^{3-}$ in the left cell.

Polarization test.

The polarization of the alkaline zinc-iron flow battery at different state of charge (SOC: 20%, 50% and 80%) using SPEEK or Nafion 212 membrane was tested according to the previous report[33]. Alternating discharge current density was applied and cell voltage at each current density was recorded.

Cyclic voltammetry (CV) of alizarin red (ARS) and $Fe(CN)_6^{4-}$/$Fe(CN)_6^{3-}$.

Cyclic voltammetry (CV) experiments of alizarin red (ARS) and $Fe(CN)_6^{4-}$/$Fe(CN)_6^{3-}$ were conducted on a Gamry Multichannel System installation (Reference 3000) by using a three electrode device (reference electrode: Hg/HgO, counter electrode: graphite plate, working electrode: graphite plate with an active area of 1 cm^2 for $Fe(CN)_6^{4-}$/$Fe(CN)_6^{3-}$ couple and glassy carbon electrode with a diameter of 0.5 cm for ARS couple. The measurements were carried out at a sweeping rate of 50 mV s^{-1}.

SOC-OCV curve.

The state-of-charge (SOC) vs. open circuit voltage (OCV) data was measured by incremented charging time (150 s) at 40 mA cm^{-2}, as described in a previous report[33].

Single cell performance of AZIFB. An AZIFB was assembled by sandwiching a membrane between two carbon felt electrodes, clamped by two graphite plates. The active area of the electrode is 6×8 cm^2. The thickness of the electrode is 5 mm. The thickness of the frame is 3 mm. All of these components were fixed between two stainless

This preprint research paper has not been peer reviewed. Electronic copy available at: https://ssrn.com/abstract=3981895

steel plates. The electrolyte was cyclically pumped through the corresponding electrodes in airtight pipelines. Different electrolyte compositions and volumes were employed for different operational mode of the battery. Charge-discharge tests were conducted by ArbinBT 2000 at a constant current density ranging from 80 to 200 mA cm^{-2}. The charge process was controlled by the charge time to keep a constant charge capacity, while the discharge process was ended with the cut-off voltage of 0.1 V. The state-of-charge (SOC) vs. open circuit voltage (OCV) data was measured by incremented charging time (120.6 s) at 40 mA cm^{-2}. The polarization curves of the alkaline zinc-iron flow battery at different state of charge (SOC: 20%, 50% and 80%) using SPEEK membrane were obtained by alternating discharge current density and recording the cell voltage at each current density. The battery experiments were tested at room temperature.

Alkaline stability of the membrane. To confirm the chemical stability in alkaline electrolytes, SPEEK membrane was treated in a 5 mol L^{-1} NaOH solution at 60 ℃ for 41 days. Afterwards, the mechanical stability of the treated membrane was measured and compared it to initial mechanical stability of the membrane. The mechanical stability of the treated and fresh SPEEK membranes (wet membrane) with a fixed sized of 1 cm × 7 cm was performed on a material test-machine (AG-2004, Shimadzu) at a loading velocity of 5 cm min^{-1}. Each result was an average value of three parallel tests.

To further investigate the alkaline stability of the SPEEK membrane, ^{1}H-NMR was performed on the treated and fresh SPEEK membrane, and the NaOH solution that used to treat the membrane. ^{1}H-NMR spectra of treated and fresh SPEEK membrane were recorded on a BRUKERDRX 700 MHz (AVAVCE III HD 700MHz) with DMSO-d_6 as the solvent and tetramethylsilane (TMS) as the internal standard. ^{1}H-NMR spectra of the NaOH solution that used to treat the SPEEK membrane (diluted to 150 mmol L^{-1}) was recorded on a BRUKERDRX 700 MHz (AVAVCE III HD 700MHz) with D_2O as the solvent. ^{1}H-NMR spectra of the NaOH solution that used to treat the SPEEK membrane (diluted to 0.5 mol L^{-1} and 1.0 mol L^{-1}) were recorded on a BRUKERDRX 400 MHz (AVANCE III 400 MHz) with D_2O as the solvent.

The long-term durability experiment of AZIFB operating at a constant current density of 80 to 160 mA cm^{-2}, was performed on the treated membrane to further verify the chemical stability of the SPEEK membrane. The battery was charging for 30 mins at 80 mA cm^{-2} and 30 mins at 160 mA cm^{-2}, respectively, endowing the battery with areal capacity of 40 mAh cm^{-2} and 80 mAh cm^{-2}, respectively. 120 mL 0.8 mol L^{-1} $Na_4Fe(CN)_6$ in 3 mol L^{-1} KOH and 120 mL 0.4 mol L^{-1} $Na_2Zn(OH)_4$ in 3 mol L^{-1} NaOH were used as positive and negative electrolyte, respectively for the battery working at 80 mA cm^{-2}. And 240 mL 0.8 mol L^{-1} $Na_4Fe(CN)_6$ in 3 mol L^{-1} KOH and 240 mL 0.4 mol L^{-1} $Na_2Zn(OH)_4$ in 3 mol L^{-1} NaOH were used as positive and negative electrolyte, respectively for the battery working at 160 mA cm^{-2}.

Single cell performance of alkaline quinone-iron flow battery. An alkaline quinone-iron flow battery was assembled by sandwiching a membrane between two carbon felt electrodes, clamped by two graphite plates. The active area of the electrode is 3×3 cm^2. All of these components were fixed between two stainless steel plates. The electrolyte was cyclically pumped through the corresponding electrodes in airtight pipelines. The electrolytes for positive and negative sides are 10 mL 0.2 mol L^{-1} $Na_4Fe(CN)_6$ in 1 mol L^{-1} KOH solution and 10 mL 0.1 mol L^{-1} alizarin red (ARS, one anthraquinone molecule) in 1.2 mol L^{-1} KOH solution, respectively. Charge-discharge cycling experiments were performed by using ArbinBT 2000 at constant current density varying from 20 to 80 mA cm^{-2} in a high purity argon filled glove box. The cut-off voltages for charging-discharging of the battery were fixed at 1.7 V and 0.4 V, respectively.

Alkaline zinc-iron flow battery stacks. To verify the practicability of SPEEK membrane in alkaline medium, alkaline zinc-iron flow battery stacks were assembled and tested by using the large-area SPEEK membrane.

The first 300 W stack was constructed by pressing 5 alkaline zinc-iron single cells together. The effective electrode area of each single cell was 875 cm^2. Each single cell was composed of two carbon felt electrodes at each side separated by a SPEEK membrane, homemade carbon plastic bipolar plates, PVC frames and gaskets. Solutions consisting of 20 L 0.8 mol L^{-1} $Fe(CN)_6^{4-}$ and 0.4 mol L^{-1} $Zn(OH)_4^{2-}$ were used as the positive and negative active materials, respectively. The stack was charged at 40 mA cm^{-2} for 1 h and discharged at 40 mA cm^{-2} with a cut-off voltage of 4 V.

This preprint research paper has not been peer reviewed. Electronic copy available at: https://ssrn.com/abstract=3981895

The second 1000 W stack was constructed by pressing 10 alkaline zinc-iron single cells together, with a similar structure to that of the first stack. The effective electrode area of each single cell was 1000 cm^2. Solutions consisting of 60 L 0.8 mol L^{-1} $Na_4Fe(CN)_6$ in 3 mol L^{-1} KOH and 60 L 0.6 mol L^{-1} $Na_2Zn(OH)_4$ in 4 mol L^{-1} NaOH were used as positive and negative electrolyte, respectively. The stack was charged at 80 mA cm^{-2} for 1 h and discharged at 80 mA cm^{-2} with a cut-off voltage of 8 V.

The third stack for long-duration energy storage was constructed by pressing 3 alkaline zinc-iron single cells together, with a similar structure to that of the second stack. The effective electrode area of each single cell was 1000 cm^2. Solutions consisting of 60 L 0.8 mol L^{-1} $Na_4Fe(CN)_6$ in 3 mol L^{-1} KOH and 60 L 0.6 mol L^{-1} $Na_2Zn(OH)_4$ in 4 mol L^{-1} NaOH were used as positive and negative electrolyte, respectively. The stack was charged at 40 mA cm^{-2} for 6 h and discharged at 40 mA cm^{-2} with a cut-off voltage of 2.4 V, and then discharged at 20 mA cm^{-2} with a cut-off voltage of 2.4 V.

The fourth 4000 W stack was constructed by pressing 15 alkaline zinc-iron single cells together, with a similar structure to that of the second stack. The effective electrode area of each single cell was 2000 cm^2. Solutions consisting of 120 L 0.9 mol L^{-1} $Na_4Fe(CN)_6$ in 3 mol L^{-1} KOH and 100 L 0.6 mol L^{-1} $Na_2Zn(OH)_4$ in 4 mol L^{-1} NaOH were used as positive and negative electrolyte, respectively. The stack was charged at 80 mA cm^{-2} for 45 mins and discharged at 80 mA cm^{-2} with a cut-off voltage of 12 V.

Data availability

The data that support the findings of this study are available from the corresponding author upon request.

References

33 Yuan, Z. *et al.* Negatively charged nanoporous membrane for a dendrite-free alkaline zinc-based flow battery with long cycle life. *Nature Communications* **9**, 3731, (2018).

40 Robertson, G. P. *et al.* Casting solvent interactions with sulfonated poly(ether ether ketone) during proton exchange membrane fabrication. *Journal of Membrane Science* **219**, 113-121, (2003).

41 Huang, R. Y. M., Shao, P., Burns, C. M. & Feng, X. Sulfonation of poly(ether ether ketone)(PEEK): Kinetic study and characterization. *Journal of Applied Polymer Science* **82**, 2651-2660 (2001).

42 Gaussian 16 Rev. A.03 (Wallingford, CT, 2016).

43 Zhao, Y. & Truhlar, D. G. Exploring the Limit of Accuracy of the Global Hybrid Meta Density Functional for Main-Group Thermochemistry, Kinetics, and Noncovalent Interactions. *J. Chem. Theory Comput.* **4**, 1849-1868, (2008).

44 Weigend, F. & Ahlrichs, R. Balanced basis sets of split valence, triple zeta valence and quadruple zeta valence quality for H to Rn: Design and assessment of accuracy. *Phys. Chem. Chem. Phys.* **7**, 3297-3305, (2005).

45 Grimme, S. Density functional theory with London dispersion corrections. *Wiley Interdisciplinary Reviews: Computational Molecular Science* **1**, 211-228, (2011).

46 Grimme, S. Accurate description of van der Waals complexes by density functional theory including empirical corrections. *J. Comput. Chem.* **25**, 1463-1473, (2004).

47 Lu, T. & Chen, F. Multiwfn: A multifunctional wavefunction analyzer. *J. Comput. Chem.* **33**, 580-592, (2012).

48 Humphrey, W., Dalke, A. & Schulten, K. VMD: Visual molecular dynamics. *Journal of Molecular Graphics* **14**, 33-38, (1996).

49 Chen, L. *et al.* Distance measurement between a spin-1/2 and a half-integer quadrupolar nuclei by solid-state NMR using exact analytical expressions. *J Magn Reson* **206**, 269-273, (2010).

50 Dai, Q. *et al.* Thin-film composite membrane breaking the trade-off between conductivity and selectivity for a flow battery. *Nature Communications* **11**, 2609, (2020).

51 Chen, J. *et al.* Ultrathin and Robust Silk Fibroin Membrane for High-Performance Osmotic Energy Conversion. *ACS Energy Letters* **5**, 742-748, (2020).

52 Xie, G. & Okada, T. The state of water in Nafion 117 of various cation forms. *Denki Kagaku* **64**, 718-

This preprint research paper has not been peer reviewed. Electronic copy available at: https://ssrn.com/abstract=3981895

726, (1996).

Acknowledgements

The authors greatly acknowledge the financial support from NSFC (21925804, 22078313, 21908214, 21773230 and 91945302), CAS Engineering Laboratory for Electrochemical Energy Storage, Liao Ning Revitalization Talents Program (XLYC1807207), DICP funding (DICP ZZBS201814), Youth Innovation Promotion Association CAS (2019182), and DNL Cooperation Found, CAS (DNL201910). Q.S. acknowledges the support from the European Research Council (ERC) under the European Union's Horizon 2020 research and innovation programme (ERC Starting Grant, grant agreement No 851272, NanoMMES).

Author contributions

Z. Z. Yuan performed the experiment, analyzed the data and written the manuscript. L. X. Liang performed the NMR experiments. Q. Dai, T. Y. Li, G. J. Hou and H. M. Zhang participated in discussion of the results. Q.S. discussed the results and edited the manuscript. X. F. Li. participated in project planning and discussions of the results and revised the manuscript. All authors reviewed the manuscript.

Competing interests

Authors declare no competing interests.

Preprint not peer reviewed

This preprint research paper has not been peer reviewed. Electronic copy available at: https://ssrn.com/abstract=3981895

Low-cost hydrocarbon membrane enables commercial-scale alkaline-based flow batteries for long-duration energy storage

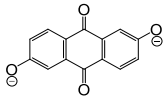
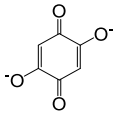
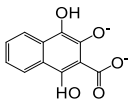
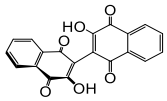
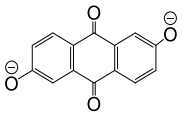
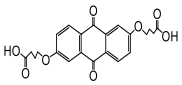
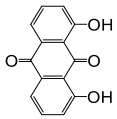
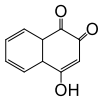
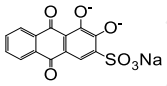
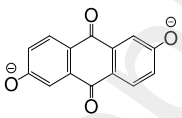
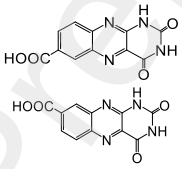
Zhizhang Yuan[1,5], Lixin Liang[2,3,5], Qing Dai[1,3], Tianyu Li[1], Qilei Song[4], Huamin Zhang[1], Guangjin Hou[2] and Xianfeng Li[1]*

[1]Division of Energy Storage, Dalian National Laboratory for Clean Energy (DNL), Dalian Institute of Chemical Physics, Chinese Academy of Sciences, Dalian, China.
[2]State Key Laboratory of Catalysis, Dalian National Laboratory for Clean Energy (DNL), Dalian Institute of Chemical Physics, Chinese Academy of Sciences, Dalian, China.
[3]University of Chinese Academy of Sciences, Beijing, China.
[4]Barrer Centre, Department of Chemical Engineering, Imperial College London, London, UK.
[5]These authors contributed equally: Zhizhang Yuan and Lixin Liang.
*Correspondence to: X. F. Li (lixianfeng@dicp.ac.cn)

Preprint not peer reviewed

This preprint research paper has not been peer reviewed. Electronic copy available at: https://ssrn.com/abstract=3981895

Supplementary information Table 1. Efficiencies of recently reported alkaline-based flow batteries using different membranes.

Negative	Positive	Supporting electrolyte	Membrane	Current density (mA cm^{-2})	Efficiencies	Cycles	Refs
			Nafion 212	100	CE~99% EE~84%	100	1
			Nafion 115 Nafion 117 Nafion 212	100	Nafion 115： CE~99% EE~65% Nafion 117 CE~99% EE~56%	150	2
			Nafion 212	100	CE~100% EE~69%	100	3
		1 mol L^{-1} KOH	Fumasep E620 K	100	CE~99% EE~77%	＜300	4
	$Fe(CN)_6^{3-}$ /$Fe(CN)_6^{4-}$		SPPO	60	CE~99% EE~83%	500	5
			Fumasep E-620 (K)	100	CE~99%	250	6
			Nafion 212	80	CE~99% EE~77%	100	7
			Nafion 117	100	CE~99% EE~55%	200	8
			PES porous membrane	80	CE~99% EE~76%	140	9
		2 mol L^{-1} KOH	SPEEK	250	CE~99% EE~66%	100	10
		2.5 mol L^{-1} KOH	Nafion 212	100	CE~99% EE~63%	400	11
$Zn(OH)_4^{2-}$/Zn	I_3^-/I^-	6 mol L^{-1} KOH (anolyte)	Nafion 117	10	CE~100% EE~80%	70	12

Preprint not peer reviewed

This preprint research paper has not been peer reviewed. Electronic copy available at: https://ssrn.com/abstract=3981895

$Zn(OH)_4^{2-}/Zn$	Fe^{2+}/Fe^{3+}	2.4 mol L^{-1} NaOH (anolyte); 1 mol L^{-1} HCl (catholyte)	Nafion 212 FAA-3 (FuMA-Tech GmbH, 45 μm)	80	CE~100% EE~76%	20	[13]

Preprint not peer reviewed

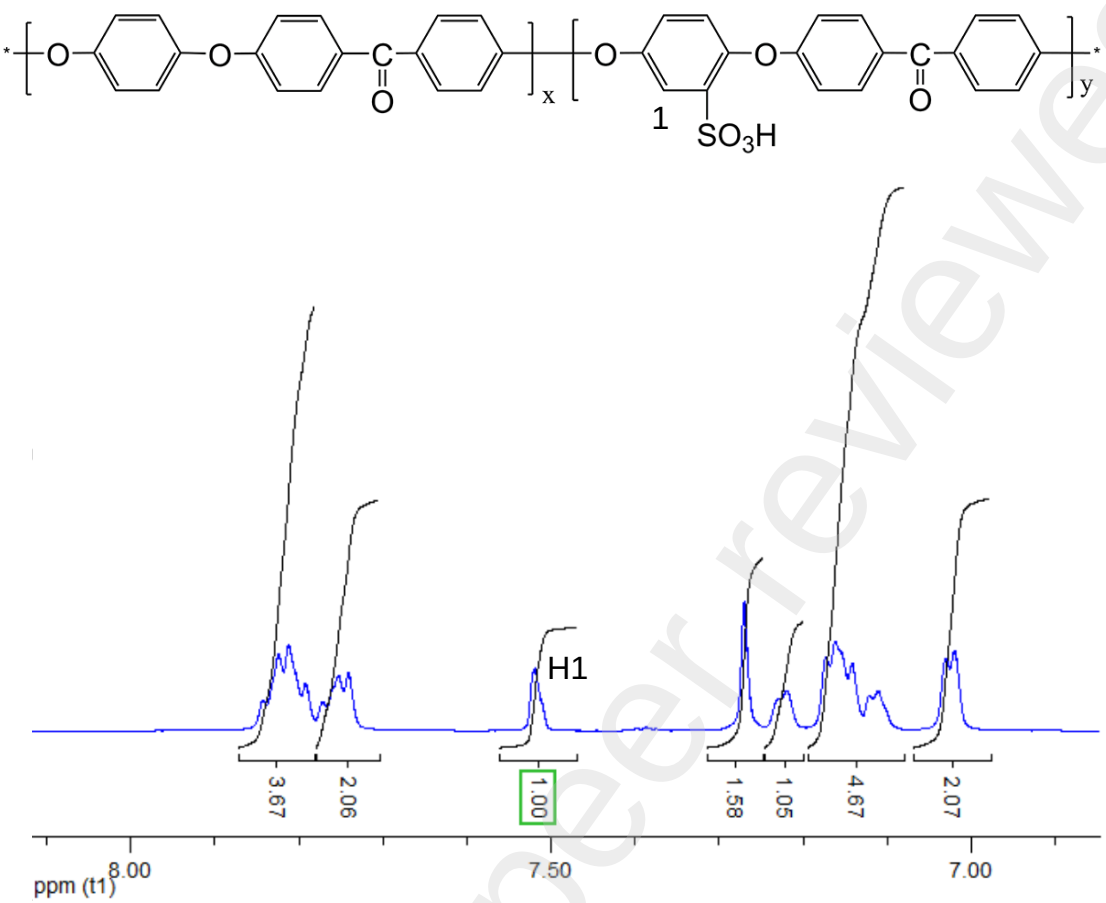
This preprint research paper has not been peer reviewed. Electronic copy available at: https://ssrn.com/abstract=3981895

Supplementary information Table 2. The key parameters and corresponding values for ranking of properties of SPEEK and Nafion membranes. The ionic conductivity, cost-effectiveness, tensile strength, alkaline stability and swelling were ranking according to the experimental results. The parameters of sustainability, safety and processability were ranking according to the membrane fabrication process. Each parameter was ranking from 1-5.

Parameters	SPEEK	Nafion
Ionic conductivity	4	2
Cost-effectiveness	5	1
Tensile strength	4	3
Sustainability	4	1
Alkaline stability	4	5
Swelling	3	4
Safety	4	2
Processability	5	4

Preprint not peer reviewed

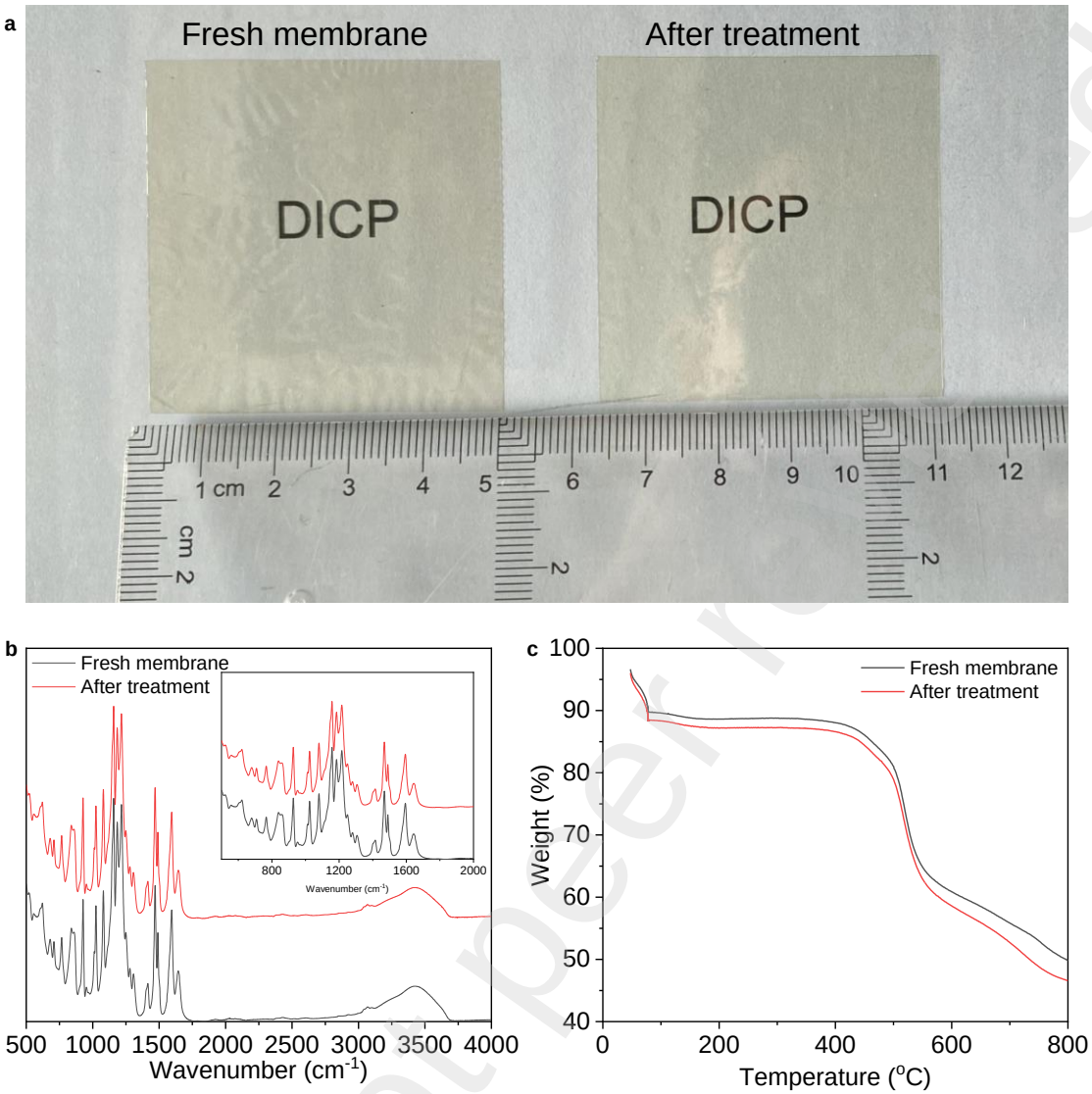
This preprint research paper has not been peer reviewed. Electronic copy available at: https://ssrn.com/abstract=3981895



Supplementary Figure 1. ^{1}H NMR spectra of SPEEK in DMSO-d_6.

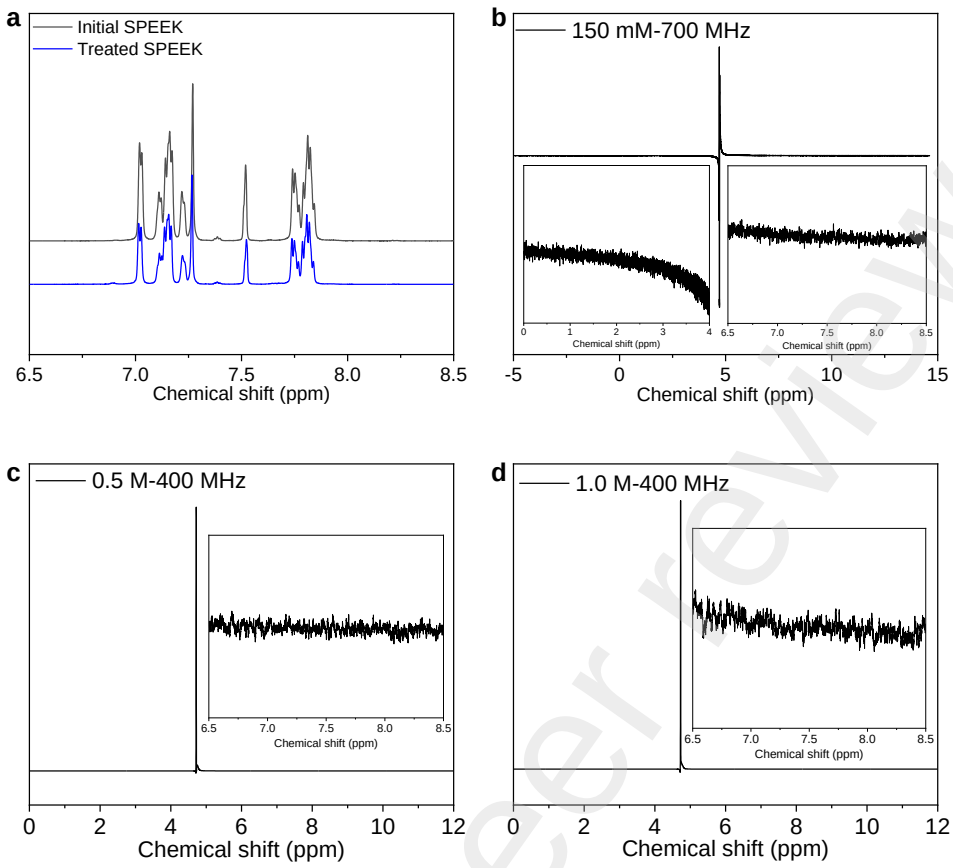
Preprint not peer reviewed

This preprint research paper has not been peer reviewed. Electronic copy available at: https://ssrn.com/abstract=3981895



Supplementary Figure 2. SPEEK membrane before and after alkaline treatment (the membrane was treated in 5 mol L^{-1} NaOH solution at 60 °C for 41 days). a, Photo of the SPEEK membrane before and after alkaline treatment. **b**, FTIR spectra and **c**, thermogravimetric analysis (TGA) of SPEEK membrane before and after alkaline treatment.

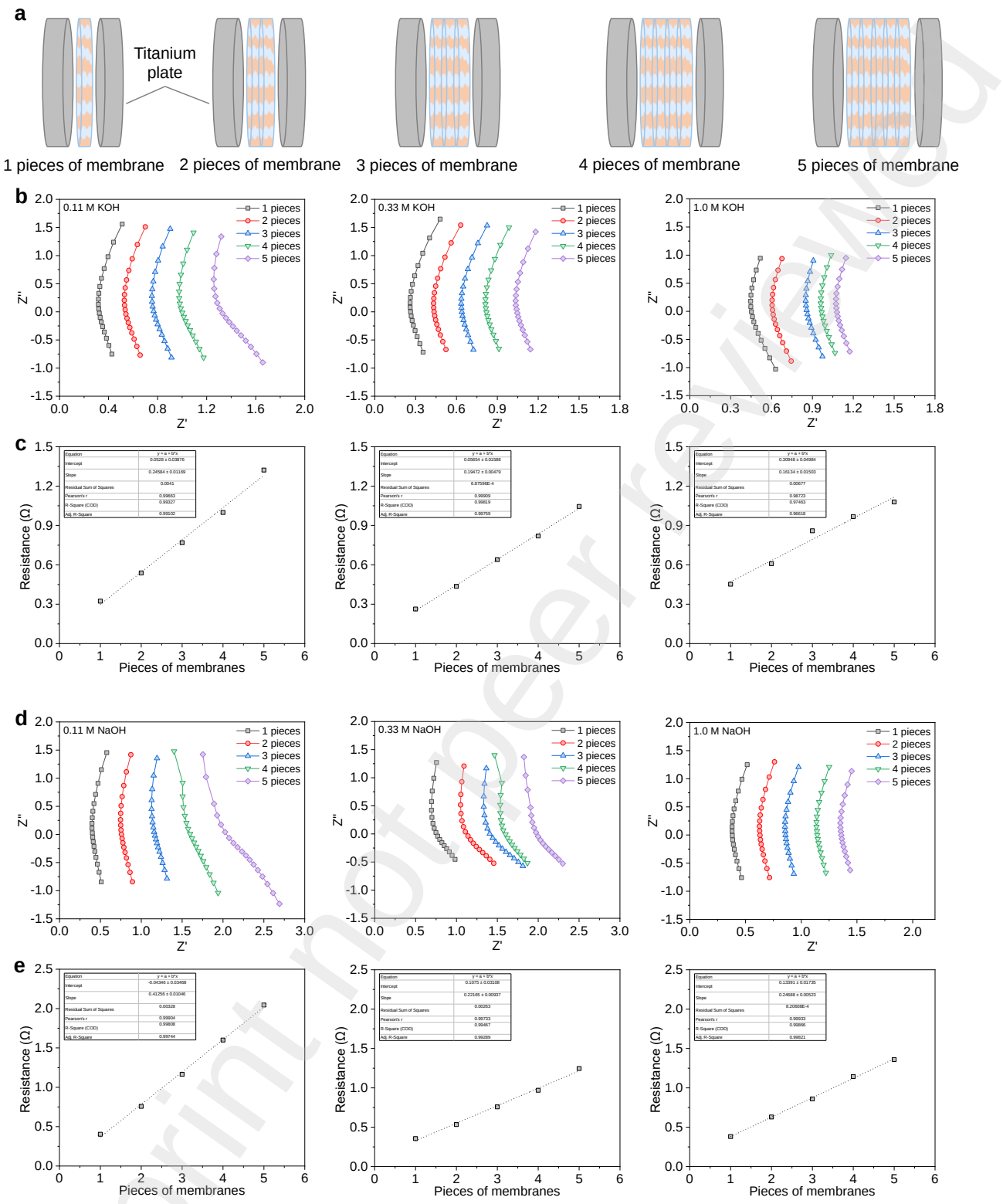
This preprint research paper has not been peer reviewed. Electronic copy available at: https://ssrn.com/abstract=3981895



Supplementary Figure 3. Chemical stability of SPEEK membrane in alkaline media. a, ^{1}H NMR spectra (performed on a Bruker 700M (AVAVCE III HD 700MHz) device) of SPEEK membrane before and after treating the membrane in 5 mol L^{-1} NaOH solution at 60 ^{o}C for 41 days. **b**, ^{1}H NMR spectra (performed on a Bruker 700M (AVAVCE III HD 700MHz) device) of the alkaline solution (5 mol L^{-1} NaOH solution used for treating the membrane at 60 ^{o}C for 41 days) diluted to 150 mmol L^{-1}. **c**, ^{1}H NMR spectra (performed on a Bruker 400M (AVANCE III 400 MHz) device) of the alkaline solution (5 mol L^{-1} NaOH solution used for treating the membrane at 60 ^{o}C for 41 days) diluted to 0.5 mol L^{-1}. **d**, ^{1}H NMR spectra (performed on a Bruker 400M (AVANCE III 400 MHz) device) of the alkaline solution (5 mol L^{-1} NaOH solution used for treating the membrane at 60 ^{o}C for 41 days) diluted to 1.0 mol L^{-1}.

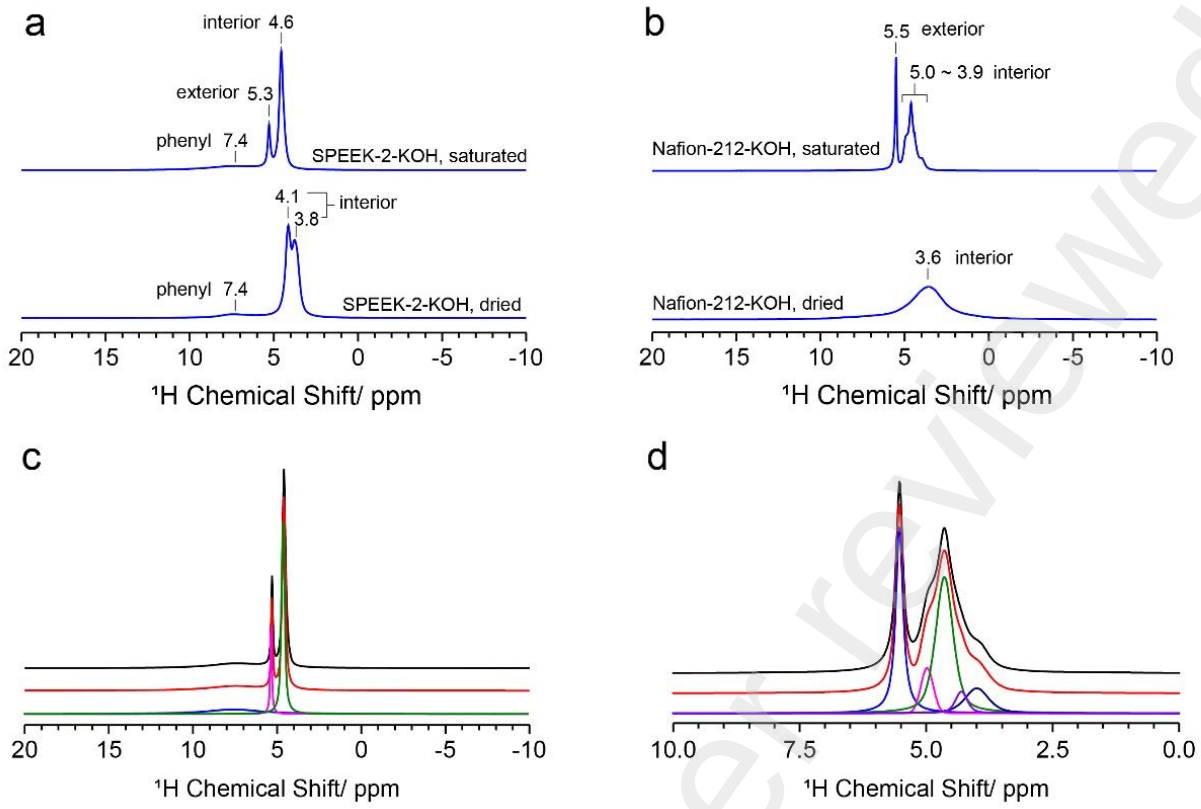
Preprint not peer reviewed

This preprint research paper has not been peer reviewed. Electronic copy available at: https://ssrn.com/abstract=3981895



Supplementary Figure 4. The SPEEK membrane resistance measured by EIS in alkaline media. a, Schematic diagram for membrane resistance measurement. **b**, The EIS plot of different pieces of SPEEK stacked layer-by-layer in KOH solution with different concentrations. **c**, The linear relation between the resistance and pieces of membranes fitted according to panel a. **d,** The EIS plot of different pieces of SPEEK stacked layer-by-layer in NaOH solution with different concentrations. **e**, The linear relation between the resistance and pieces of membranes fitted according to panel c. The resistance for one pieces of membrane was calculated from the slope of the linear fit of the resistance vs. the pieces of membranes stacked layer-by-layer.

This preprint research paper has not been peer reviewed. Electronic copy available at: https://ssrn.com/abstract=3981895



Supplementary Figure 5. NMR spectra of SPEEK and Nafion 212 membranes. The ^{1}H NMR spectra of **a**, SPEEK-2-KOH and **b**, Nafion-212-KOH, and the **c** and **d** are deconvolutions of ^{1}H NMR spectra of wet samples, respectively.

In the as-prepared wet samples (SPEEK or Nafion 212 swollen in 3 mol L^{-1} KOH solution), the KOH solution remaining on the surface resulted in isotropic chemical shifts ($\delta_{iso}(^{1}H)$) at 5.3 ppm for SPEEK-KOH and 5.5 ppm for Nafion 212-KOH. These signals from exterior water vanished after drying the samples in air at 30% humidity for 9 hours (Fig. 3g in the main article), which was consistent with a previous report[14]. For both samples, the $\delta_{iso}(^{1}H)$ of interior water-related species (H_2O, OH^-, etc.) was sensitive to the water content, ranging from 3.5~5.0 ppm, and the $\delta_{iso}(^{1}H)$ of the phenyl proton in SPEEK-KOH was 7.4 ppm, as shown in projection spectra in Fig. 3g and 3j in the main article, as well as Supplementary information Fig. S5a.

The ^{1}H NMR revealed significantly different dynamic behavior of protons for water-relating species in SPEEK-KOH and Nafion 212-KOH. The slow proton exchange, among interior protons and between exterior and interior protons, was further identified by the absence of cross peaks in 2D ^{1}H-^{1}H EXSY shown in Fig. 3j in the main article. Besides, the ^{1}H peaks of water-relating species of SPEEK-KOH were narrower than those of Nafion 212-KOH, suggesting higher proton mobility, as revealed by the analysis of spin-spin relaxation time (T_2) (Supplementary information Table S3).

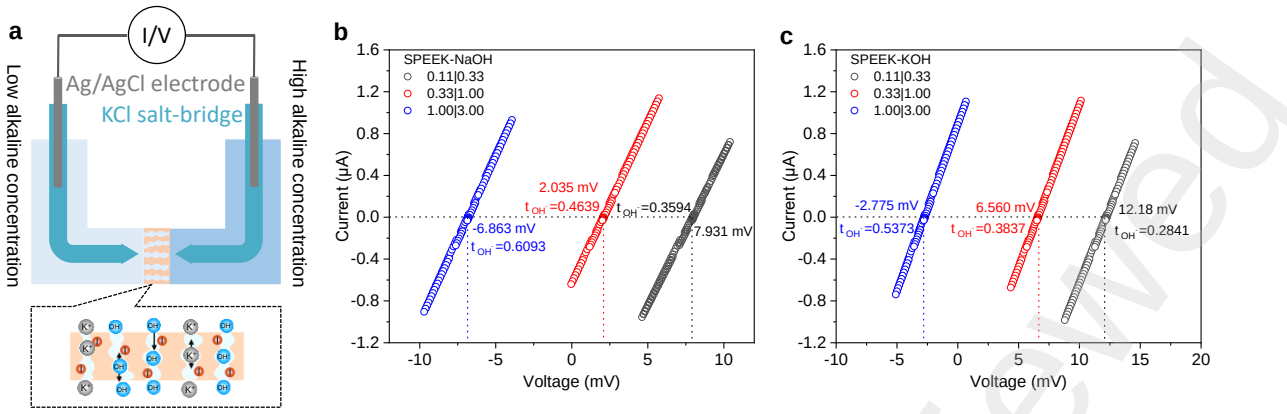
On the other hand, the ^{17}O NMR spectra, obtained from both samples after water exchange with 90% enriched

This preprint research paper has not been peer reviewed. Electronic copy available at: https://ssrn.com/abstract=3981895

$^{17}OH_2$, showed opposite mobility of ^{17}O atoms in SPEEK-KOH and Nafion 212-KOH, compared to the ^{1}H NMR results. With similar amount of samples (0.0257 g for SPEEK-KOH and 0.0276 g for Nafion-212-KOH) and the same 3 μl of $^{17}OH_2$ for exchange, the interior ^{17}O (at -7.9 ppm) in SPEEK-KOH exhibited a significantly broader signal (Fig. 3h) than the interior ^{17}O (at -3.8 ppm) in Nafion 212-KOH (Fig. 3k in the main article), thus a notably shorter T_2, as shown in Supplementary information Table S4. The broad ^{17}O signal was due to the strongly confined ^{17}O atomic motion which caused large quadrupolar coupling. The absence of exterior ^{17}O was consistence with the higher water capacity of SPEEK membrane. Whereas the narrower interior ^{17}O signal in Nafion-2-KOH indicated significantly less confined motion, comparable to the ^{17}O in exterior water at 1.4 ppm (Fig. 3k in the main article). Further, the existence of hydrogen bonding network in SPEEK-KOH were revealed by ^{1}H-^{17}O S-RESPDOR[15] experiments, where the dipolar coupling between the strongly confined ^{1}H and ^{17}O atoms with spatial proximity could cause the loss of ^{1}H signal intensity (S) compared to the reference spectra (S_0), as illustrated in Fig. 3i in the main article. Therefore, the close and confined ^{1}H and ^{17}O atoms indicated the existence of the hydrogen bonding network. Even saturated by $^{17}OH_2$, the loss of ^{1}H signal intensity could still be observed in the ^{1}H-^{17}O S-RESPDOR experiments (Supplementary information Fig. S9), i.e., the hydrogen bonding network still existed. In addition, as clearly demonstrated in Fig. 3i in the main article, the observation of a reduced signal of exterior water in the S-RESPDOR spectra highly suggests the existence of hydrogen-bonding networks at the interface between the SPEEK membrane and exterior solution. These hydrogen-bonding networks at the surface of the membrane could promote the transport of OH^- from the exterior solution to the membrane channel, which is in accordance with the ^{1}H exchange experiment in Fig. 3g in the main article, thus providing a high ion-conductive SPEEK membrane.

Preprint not peer reviewed

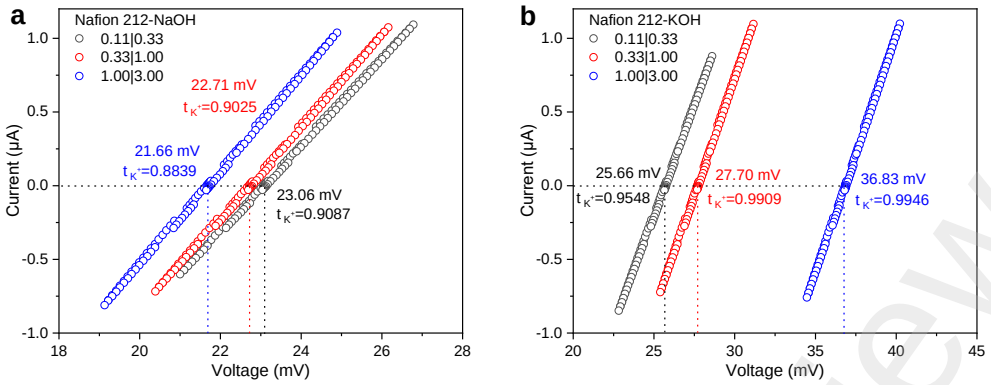
This preprint research paper has not been peer reviewed. Electronic copy available at: https://ssrn.com/abstract=3981895



Supplementary Figure 6. The voltage-current (V-I) profiles. a, Schematic illustration of V-I testing device. The cation transference numbers and OH^- transference numbers calculated from V-I profiles for different **b**, NaOH and **c**, KOH concentration gradients in the two reservoirs connected by a SPEEK membrane.

Preprint not peer reviewed

This preprint research paper has not been peer reviewed. Electronic copy available at: https://ssrn.com/abstract=3981895



Supplementary Figure 7. The voltage-current (V-I) profiles. The cation transference numbers and OH^- transference numbers calculated from V-I profiles for different **a**, NaOH and **b**, KOH concentration gradients in the two reservoirs connected by a Nafion 212 membrane.

Preprint not peer reviewed

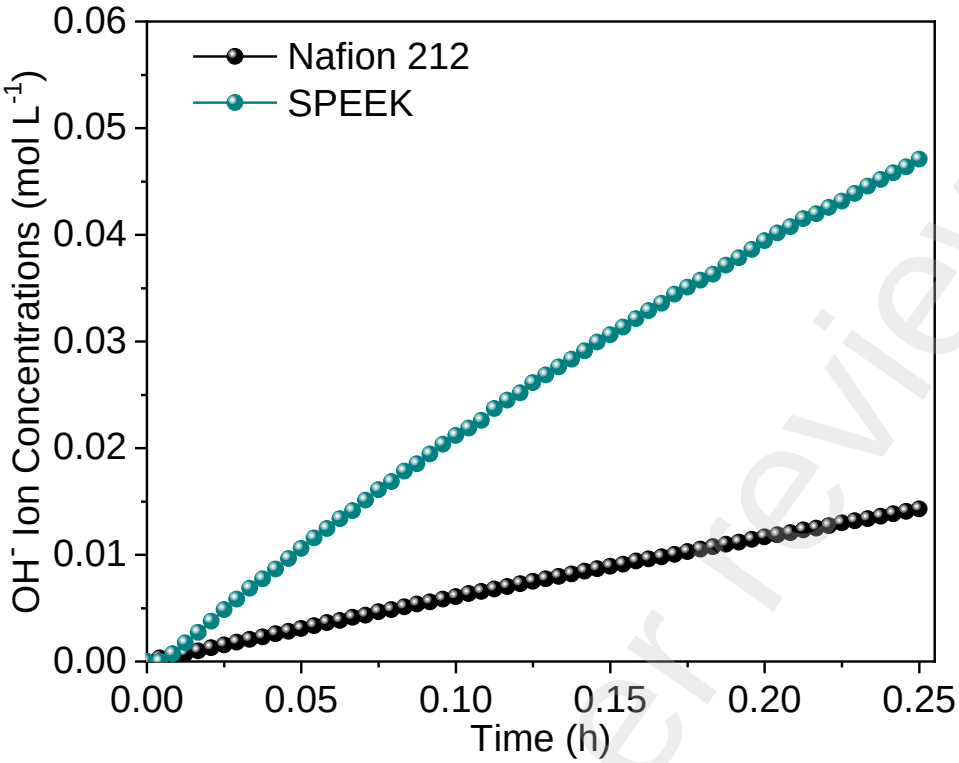
This preprint research paper has not been peer reviewed. Electronic copy available at: https://ssrn.com/abstract=3981895

Supplementary information Table 3. ^{1}H T_2 for each signal in Fig. 3g and 3j in the main article.

Sample	SPEEK-KOH			Nafion-212-KOH				
$\delta_{^1H}$/ppm	7.6	5.3	4.6	5.5	5.0	4.6	4.3	4.0
T_2/ms	0.66	23	11	15	8.6	6.1	8.9	4.5

Preprint not peer reviewed

This preprint research paper has not been peer reviewed. Electronic copy available at: https://ssrn.com/abstract=3981895



Supplementary Figure 8. The permeability of OH^- through Nafion 212 and SPEEK membranes.

Preprint not peer reviewed

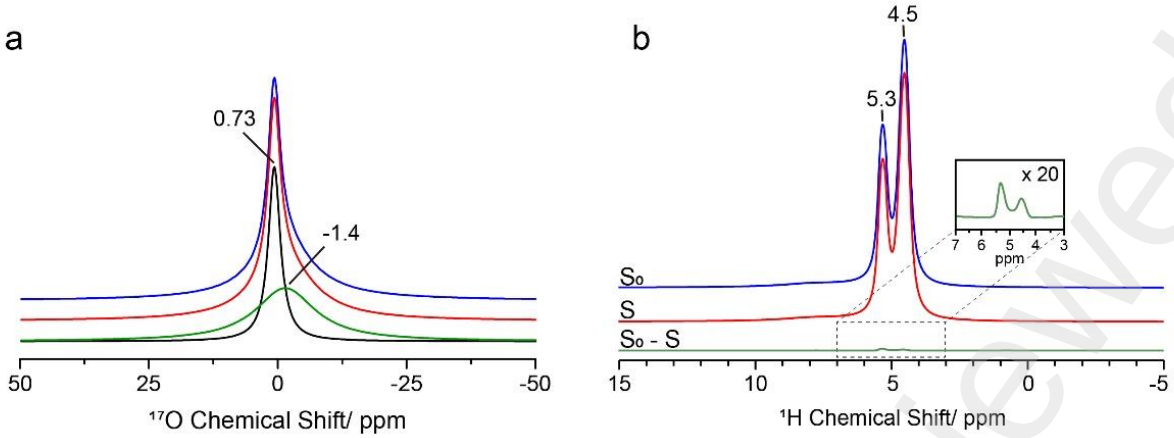
This preprint research paper has not been peer reviewed. Electronic copy available at: https://ssrn.com/abstract=3981895

Supplementary information Table 4. ^{1}H and ^{17}O T_2 of signals after rehydration.

Sample	SPEEK-KOH			Nafion-212-KOH				
$\delta_{^1H}$/ppm	7.6	4.5	4.0	5.2	4.8	4.5	4.2	4.0
T_2/ms	1.0	6.25	4.16	28	17	8.9	4.9	6.8
$\delta_{^{17}O}$/ppm		-7.9			1.4		-4.2	
T_2/ms		0.25			8.5		2.2	

Preprint not peer reviewed

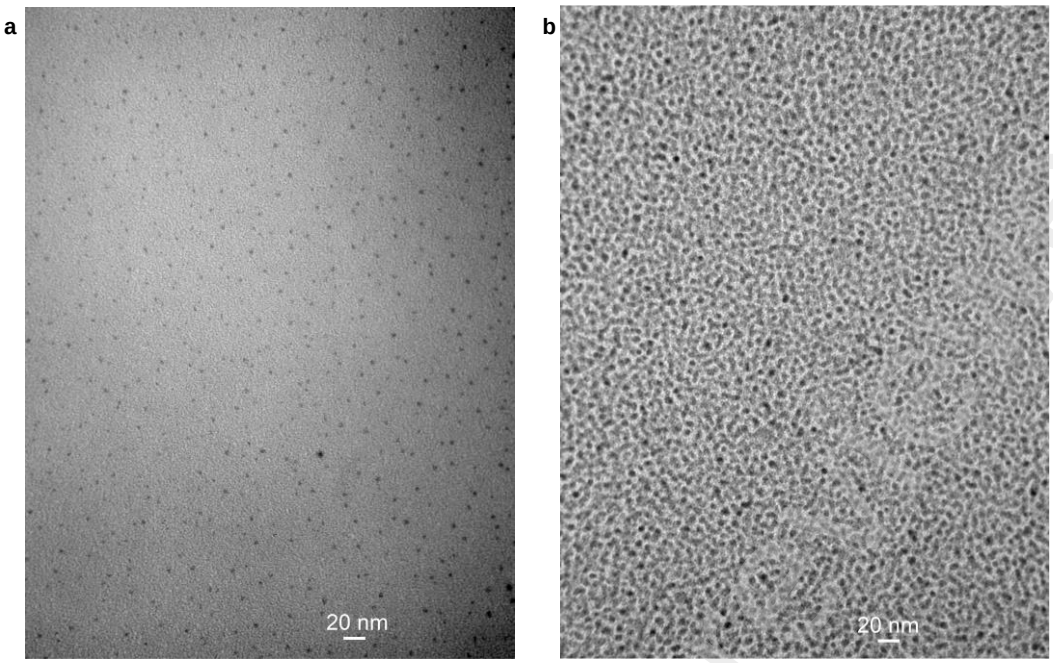
This preprint research paper has not been peer reviewed. Electronic copy available at: https://ssrn.com/abstract=3981895



Supplementary Figure 9. NMR spectra of SPEEK membrane. a, The ^{17}O NMR spectra of $^{17}OH_2$ saturated SPEEK-2-KOH and **b**, the corresponding ^{1}H-^{17}O S-RESPDOR experiments.

Preprint not peer reviewed

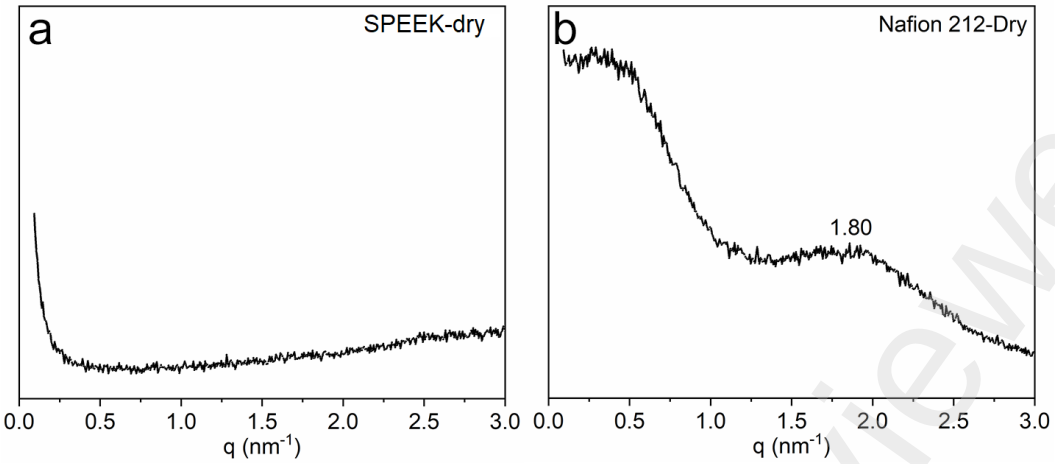
This preprint research paper has not been peer reviewed. Electronic copy available at: https://ssrn.com/abstract=3981895



Supplementary Figure 10. Distribution of –SO_3H in a, SPEEK and b, Nafion 212.

Preprint not peer reviewed

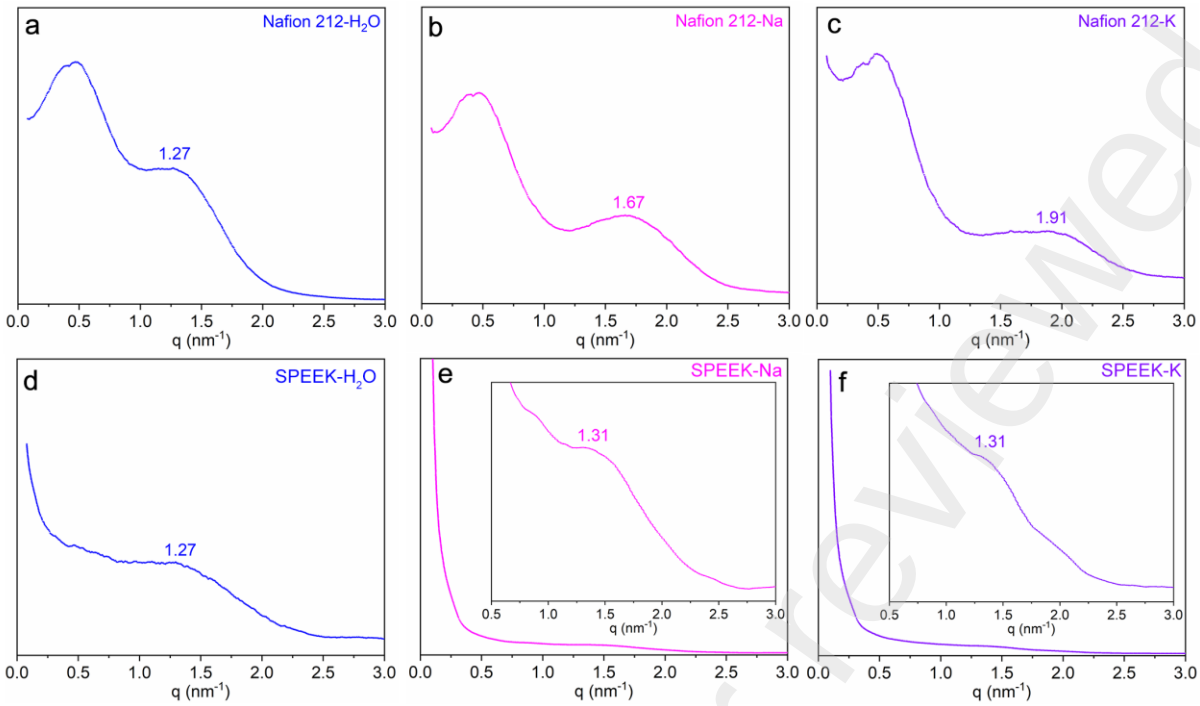
This preprint research paper has not been peer reviewed. Electronic copy available at: https://ssrn.com/abstract=3981895



Supplementary Figure 11. SAXS patterns of a, dry SPEEK and b, dry Nafion 212 membranes.

Preprint not peer reviewed

This preprint research paper has not been peer reviewed. Electronic copy available at: https://ssrn.com/abstract=3981895



Supplementary Figure 12. The SAXA patterns of the membranes. SAXS patterns of **a**, water saturated Nafion 212, **b**, 0.5 mol L^{-1} NaOH solution saturated Nafion 212, **c**, 0.5 mol L^{-1} KOH solution saturated Nafion 212 and **d**, water saturated SK-2, **e**, 0.5 mol L^{-1} NaOH solution saturated SK-2, **f**, 0.5 mol L^{-1} KOH solution saturated SK-2. The scattering ionomer peaks for the dry Nafion 212, water saturated Nafion 212, 0.5 mol L^{-1} NaOH solution saturated Nafion 212 and 0.5 mol L^{-1} KOH solution saturated Nafion 212 are found at 1.80 nm^{-1}, 1.27 nm^{-1}, 1.67 nm^{-1}, and 1.91 nm^{-1}, respectively, which corresponds to the Bragg spacing d calculated from Bragg equation of 3.49 nm, 4.95 nm, 3.76 nm and 3.29 nm, respectively.

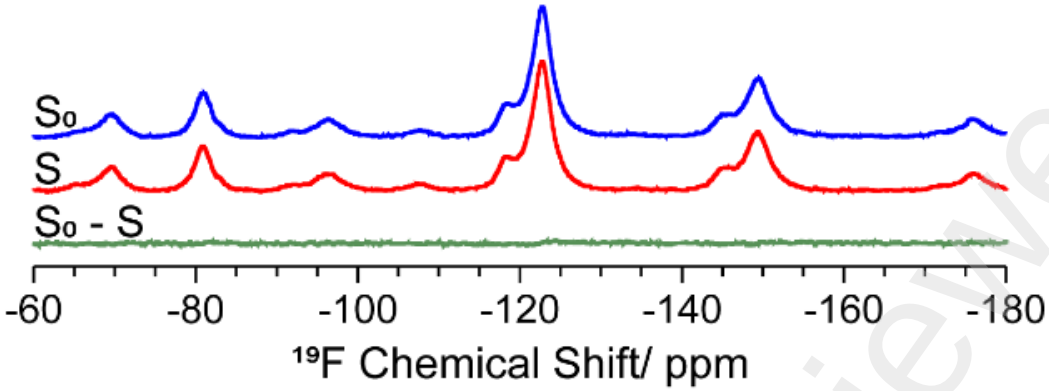
Compared with the dry Nafion 212 membrane, the Bragg spacing d (a reflection of the size of hydrophilic cluster for a membrane) for 0.5 mol L^{-1} KOH solution saturated Nafion 212 membrane decreased, indicating that the KOH solution could squeeze the Nafion 212 membrane. The squeezed hydrophilic cluster could force free water that interacts with $–SO_3H$ (or hydration shell around H^+ formed by water molecules[16]) through H-bonding to dehydrate in KOH solution, since Nafion has higher affinity for K^+ than for H^+[16]. Compared with Nafion 212 membrane, the distribution of $–SO_3H$ in SPEEK is random and dispersive, leading to no scattering ionomer peak in small-angle X-ray scattering (SAXS) profile. By contrast, the aggregation of $–SO_3H$ could be found in Nafion 212, which results in the formation of ion clusters in the membrane. Additionally, the skeleton of SPEEK is rigid and the acidity of $–SO_3H$ in SPEEK is weaker than that in Nafion membrane. Because of the rigid skeleton, the electrostatic potential on SPEEK obtained from density functional theory (DFT) calculation is considerably more uniform than that on Nafion 212. And the electrostatic potential of proton in $–SO_3H$ of SPEEK (+75.95 kcal mol^{-1}) is lower than that of proton in $–SO_3H$ of Nafion 212 (+97.95 kcal mol^{-1}), further indicating that the acidity of $–SO_3H$ in SPEEK is weaker than that in Nafion 212. This indicates that the dissociation ability of $–SO_3H$ in SPEEK is much weaker than that of the dissociation ability of $–SO_3H$ in Nafion 212. This favors the formation of continuous hydrogen-bonding network between the sulfonated groups, OH^- and the free water in the membrane and enhancing Grotthuss (hydrogen-hopping) mechanism therefore, endowing SPEEK membrane with a higher swelling and electrolyte uptake and further ionic conductivities and OH^- transference numbers, both in the NaOH and KOH solutions. In alkaline medium, K^+ and Na^+ have a higher affinity toward H^+ in $–SO_3H$ group, which results from their stronger electrostatic interaction with $–SO_3H$. Normally, the larger size of the cation has a weaker ionic hydration capacity[17]. Thus, the larger cation squeezes out the free water around the hydrophilic cluster of the membrane[18] and further lowers the

This preprint research paper has not been peer reviewed. Electronic copy available at: https://ssrn.com/abstract=3981895

swelling of the membrane[19,20] and the fraction of freezable water in the membrane[21]. This is why both SPEEK and Nafion membranes exhibit a lower swelling ratio and electrolyte uptake in KOH solution than those in NaOH solution at the same alkaline concentration.

Preprint not peer reviewed

This preprint research paper has not been peer reviewed. Electronic copy available at: https://ssrn.com/abstract=3981895

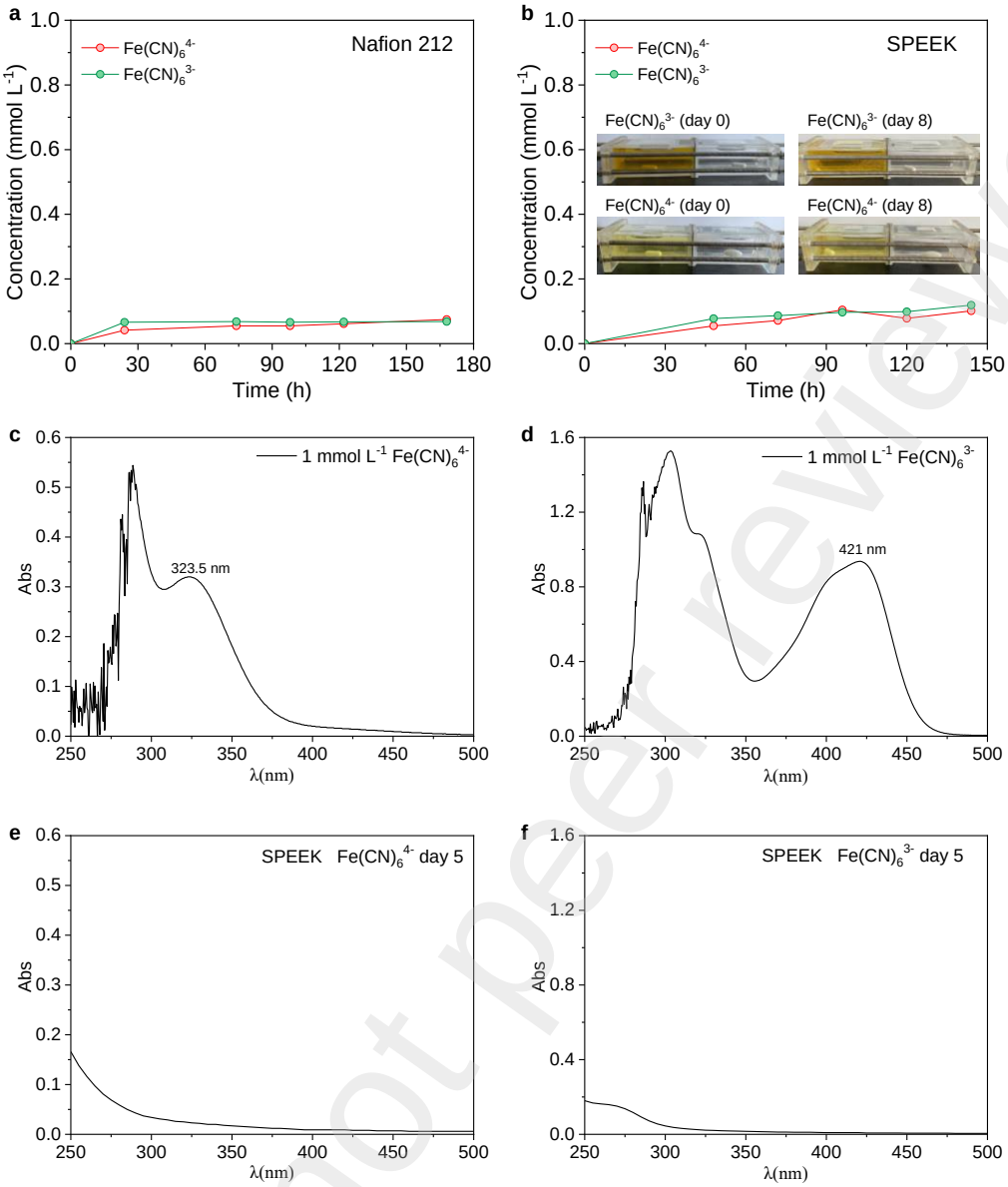


Supplementary Figure 13. NMR spectra of Nafion 212 membranes. ^{19}F-^{17}O of Nafion-212-KOH, the recoupling time of the three experiments were 0.4 ms under 10 kHz MAS.

Combing the NMR spectra in Fig. 3l and Supplementary Figure 13, it can be concluded that no obvious dipolar coupling was observed between ^{17}O and ^{1}H atoms (Fig. 3l) and between ^{17}O and the backbone ^{19}F in Nafion-212-KOH. Although the proton exchange in Nafion-212-KOH was slow, the oxygen-containing species (mainly H_2O and OH^-) experienced fast molecular motion.

Preprint not peer reviewed

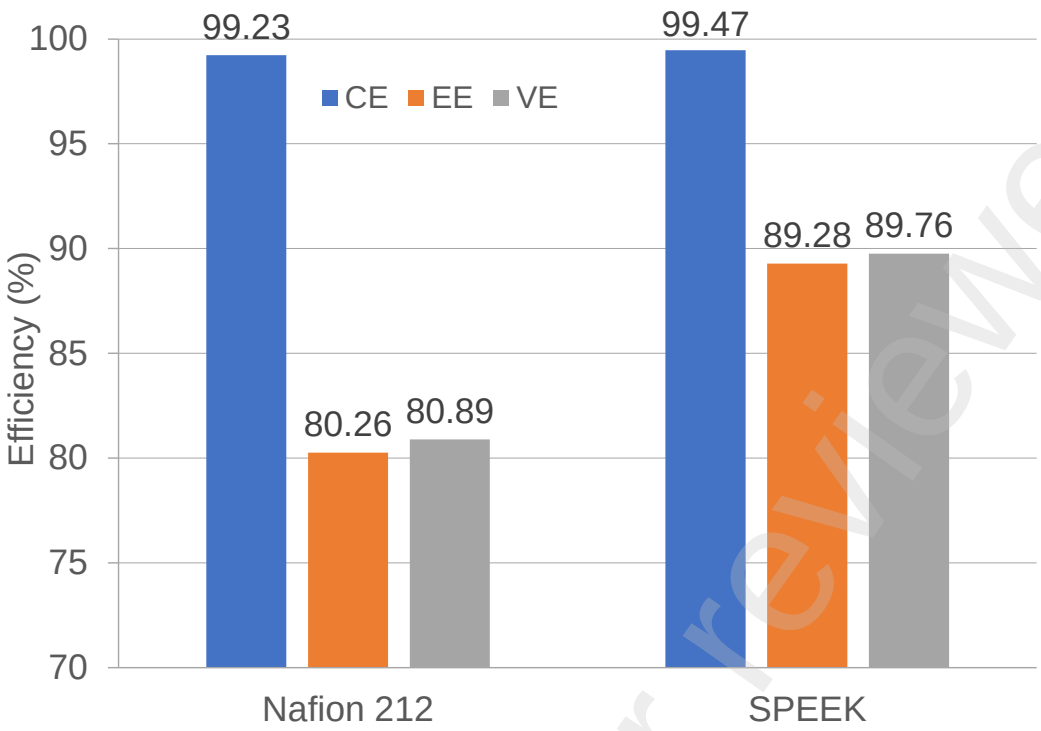
This preprint research paper has not been peer reviewed. Electronic copy available at: https://ssrn.com/abstract=3981895



Supplementary Figure 14. Permeability experiment of $Fe(CN)_6^{4-}$/$Fe(CN)_6^{3-}$ through Nafion 212 and SPEEK membranes. $Fe(CN)_6^{3-}$/$Fe(CN)_6^{4-}$ concentration versus time at the diffused side of a diffusion cell using **a**, Nafion 212 membrane, **b**, SPEEK membrane (detected by the UV-Visible spectroscopy). Inset, visual experimental of $Fe(CN)_6^{3-}$/$Fe(CN)_6^{4-}$ permeability. From the diffused side of the diffusion cell, no obviously color change could be observed, demonstrating high selectivity of the SPEEK membrane. UV-vis absorption spectrum of **c**, 1 mmol L^{-1} $Fe(CN)_6^{4-}$ in 3 mol L^{-1} alkaline solution, **d**, 1 mmol L^{-1} $Fe(CN)_6^{3-}$ in 3 mol L^{-1} alkaline solution. UV-vis absorption spectrum of **e**, sample collected from the diffusion cell ($Fe(CN)_6^{4-}$) using a SPEEK membrane at day 5, **d**, sample collected from the diffusion cell ($Fe(CN)_6^{3-}$) using a SPEEK membrane at day 5.

Preprint not peer reviewed

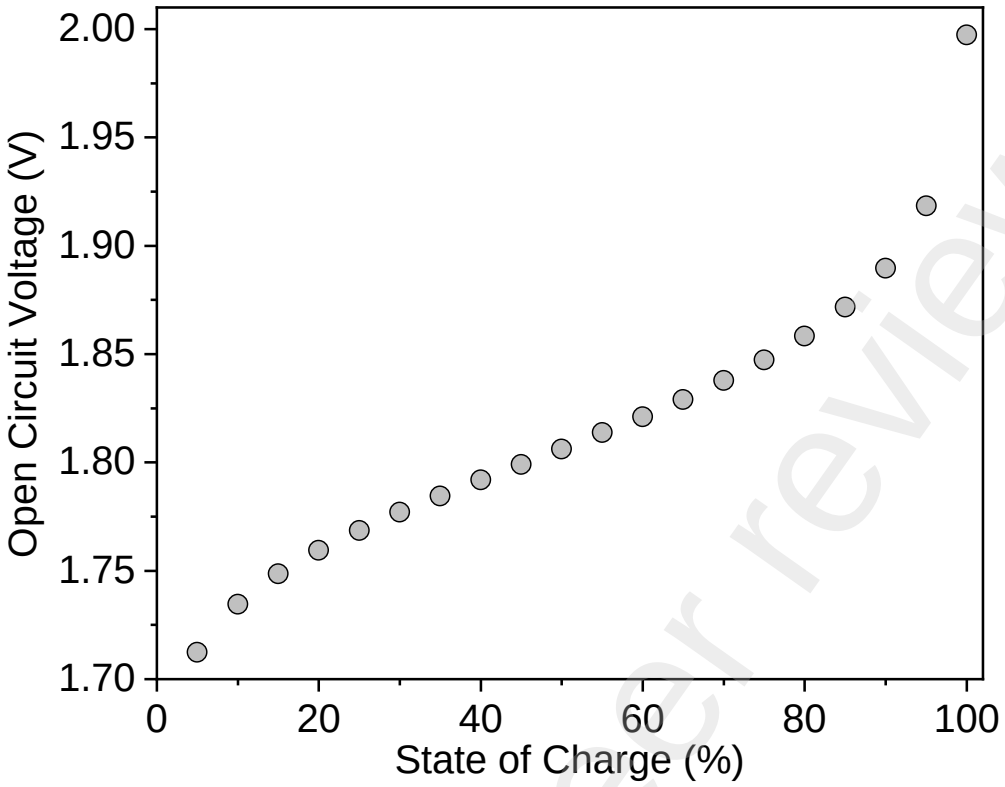
This preprint research paper has not been peer reviewed. Electronic copy available at: https://ssrn.com/abstract=3981895



Supplementary Figure 15. The efficiencies of AZIFB. Efficiencies of the AZIFB assembled with Nafion 212 and SPEEK membranes, respectively at 80 mA cm^{-2}. 60 mL 0.6 mol L^{-1} $K_4Fe(CN)_6$ + 5 mol L^{-1} NaOH and 60 mL 0.3 mol L^{-1} $Na_2Zn(OH)_4$ + 5 mol L^{-1} NaOH were used as positive and negative electrolyte, respectively.

Preprint not peer reviewed

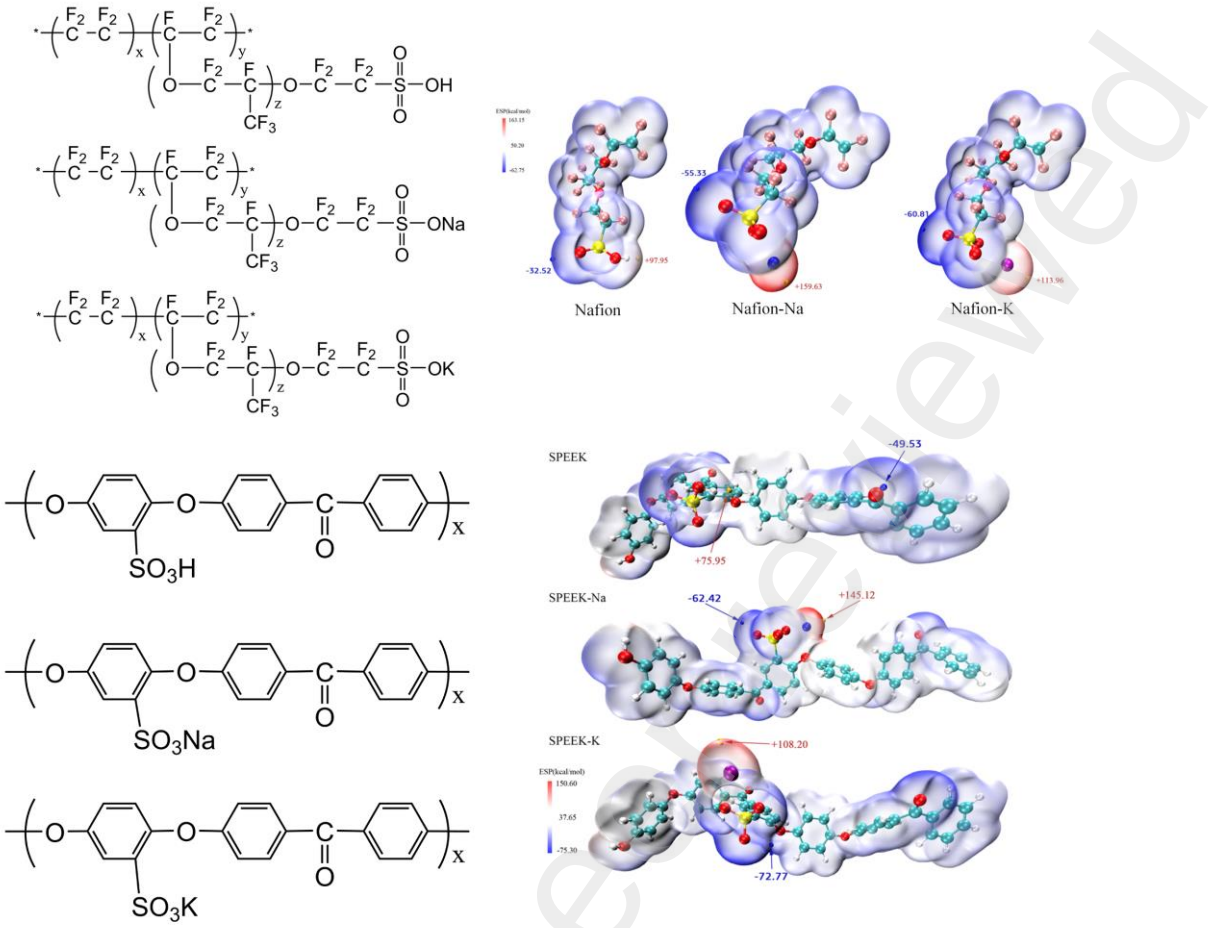
This preprint research paper has not been peer reviewed. Electronic copy available at: https://ssrn.com/abstract=3981895



Supplementary Figure S16. The open cell voltage (OCV) versus state of charge (SOC) of an alkaline zinc-iron flow battery using a SPEEK membrane.

Preprint not peer reviewed

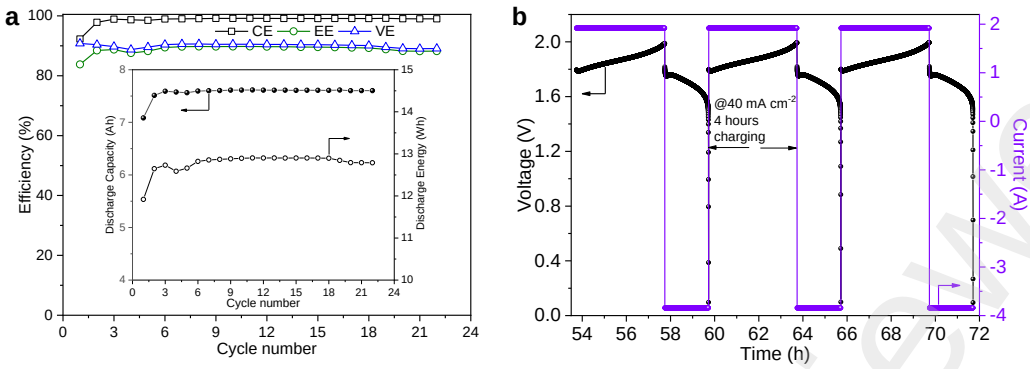
This preprint research paper has not been peer reviewed. Electronic copy available at: https://ssrn.com/abstract=3981895



Supplementary Figure 17. The ESP of the membranes. The chemical structure and electrostatic potential (ESP) on an isosurface of electronic density (0.001 a.u.) for Nafion, Nafion-Na, Nafion-K, SPEEK, SPEEK-Na, SPEEK-K, respectively.

Preprint not peer reviewed

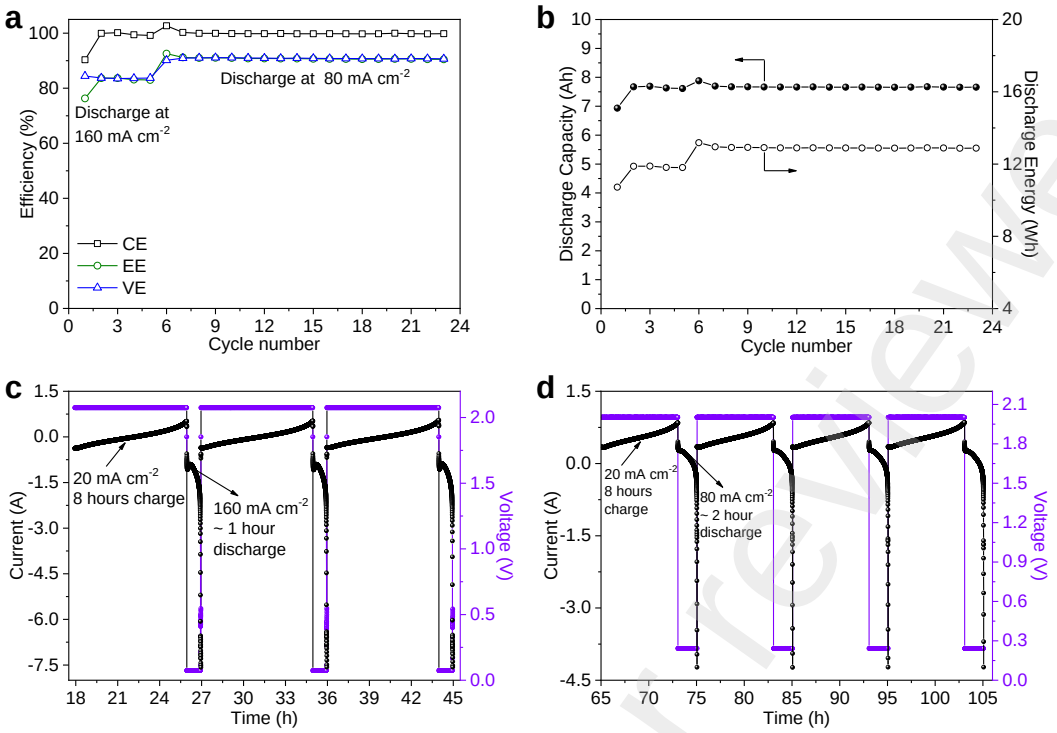
This preprint research paper has not been peer reviewed. Electronic copy available at: https://ssrn.com/abstract=3981895



Supplementary Figure 18. Performance of the single AZIFB battery. a, The performance of the AZIFB at a high areal capacity. The battery was charged for 4 hours at 40 mA cm^{-2} and discharged at 80 mA cm^{-2}. Insert, discharge capacity and discharge energy of the battery. **b**, The corresponding voltage (current)-time curves of the battery in panel **a**. 420 mL 0.8 mol L^{-1} $Na_4Fe(CN)_6$ + 3 mol L^{-1} KOH and 420 mL 0.4 mol L^{-1} $Na_2Zn(OH)_4$ + 3 mol L^{-1} NaOH were used as positive and negative electrolyte, respectively.

Preprint not peer reviewed

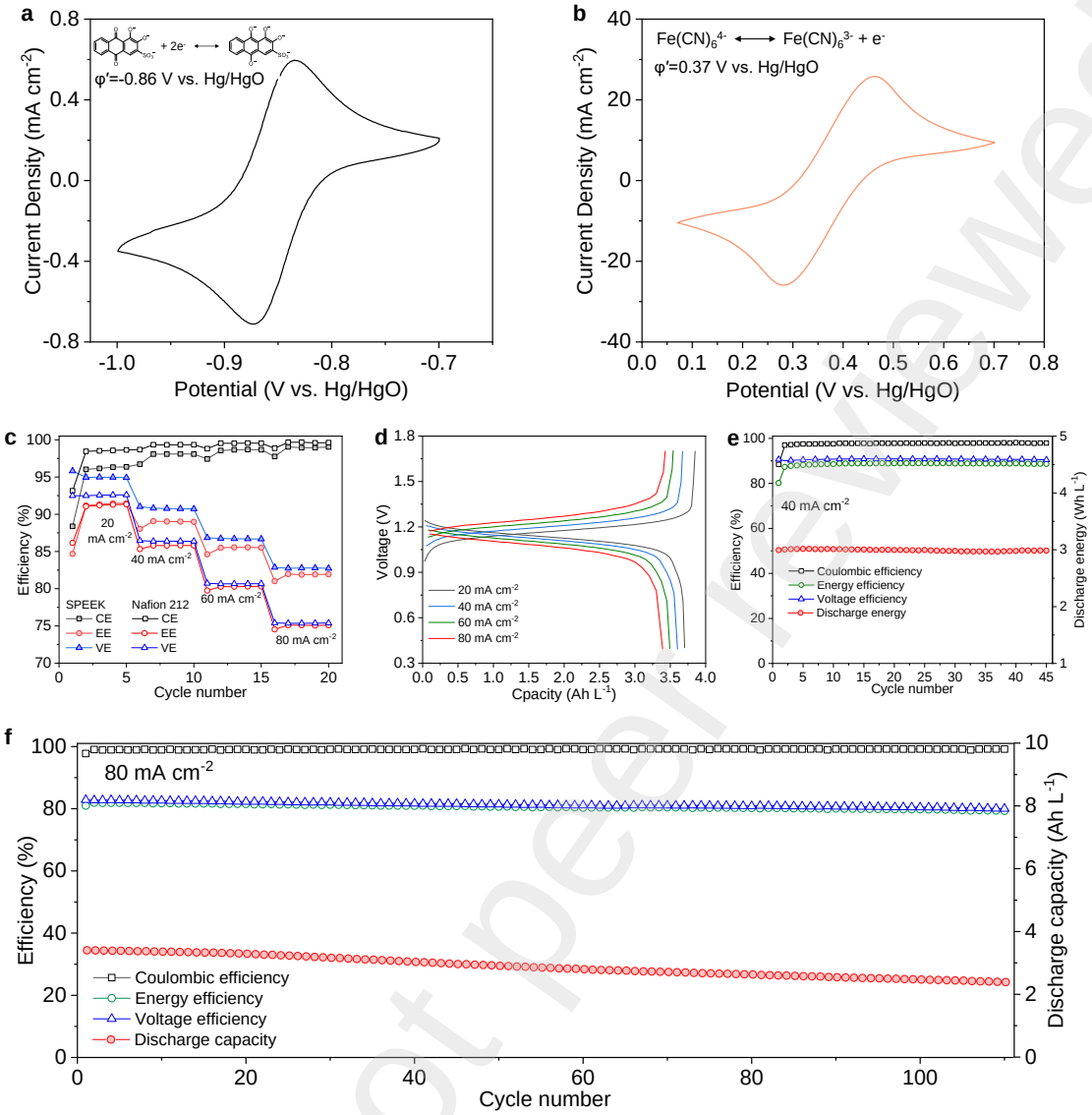
This preprint research paper has not been peer reviewed. Electronic copy available at: https://ssrn.com/abstract=3981895



Supplementary Figure 19. The performances of AZIFB assembled with a SPEEK membrane at different operational modes. a, Efficiencies of the battery. **b**, Corresponding discharge capacity and discharge energy for each cycle. **c**, Representative charge and discharge curves (160 mA cm^{-2}) of the alkaline zinc–iron flow battery. **d**, Representative charge and discharge curves (80 mA cm^{-2}) of the alkaline zinc–iron flow battery. The battery was charged for 8 hours at 20 mA cm^{-2} and discharged at 160 mA cm^{-2} and 80 mA cm^{-2}, respectively. 420 mL 0.8 mol L^{-1} $Na_4Fe(CN)_6$ + 3 mol L^{-1} KOH and 420 mL 0.4 mol L^{-1} $Na_2Zn(OH)_4$ + 3 mol L^{-1} NaOH were used as positive and negative electrolyte, respectively.

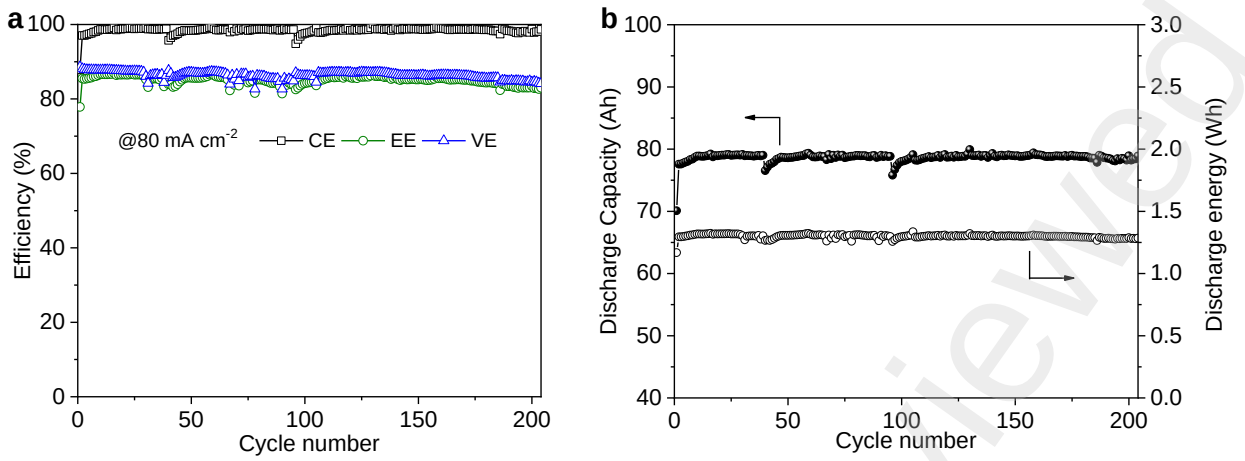
Preprint not peer reviewed

This preprint research paper has not been peer reviewed. Electronic copy available at: https://ssrn.com/abstract=3981895



Supplementary Figure 20. Single cell performance of alkaline alizarin red-iron flow battery. Cyclic voltammetry (CV) scans of **a**, 0.1 mol L^{-1} ARS in 1 mol L^{-1} KOH solution and **b**, 0.2 mol L^{-1} $Fe(CN)_6^{4-}/Fe(CN)_6^{3-}$ in 1 mol L^{-1} KOH solution at a scan rate of 50 mV s^{-1}. **c**, Efficiencies of the alkaline alizarin red-iron flow battery assembled with Nafion 212 and SPEEK at different current densities. **d**, The charge and discharge curves of the alkaline alizarin red-iron flow battery assembled with a SPEEK membrane at different current densities. **e**, The cycle performance of the alkaline alizarin red-iron flow battery assembled with SPEEK membrane at 40 mA cm^{-2}. **f**, The cycle performance of the alkaline alizarin red-iron flow battery assembled with SPEEK membrane at 80 mA cm^{-2}.

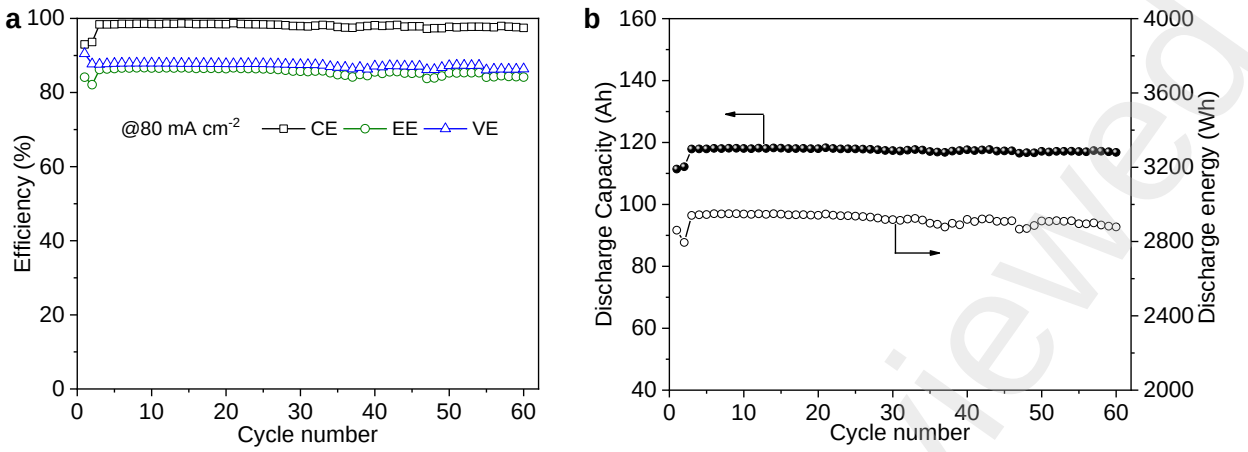
This preprint research paper has not been peer reviewed. Electronic copy available at: https://ssrn.com/abstract=3981895



Supplementary Figure 21. Performances of 1000 W AZIFB cell stack assembled with the SPEEK. a, The cycling performance of a kilowatt cell stack (10 single cells) using the designed membrane at the current density of 80 mA cm^{-2}. **b**, Discharge capacity and discharge energy of the cell stack.

Preprint not peer reviewed

This preprint research paper has not been peer reviewed. Electronic copy available at: https://ssrn.com/abstract=3981895



Supplementary Figure 22. Performances of 4000 W AZIFB cell stack assembled with the SPEEK. a, The cycling performance of a 4000 W cell stack using SK-2 at the current density of 80 mA cm^{-2}. **b**, The discharge capacity and discharge energy of the stack.

Preprint not peer reviewed

This preprint research paper has not been peer reviewed. Electronic copy available at: https://ssrn.com/abstract=3981895

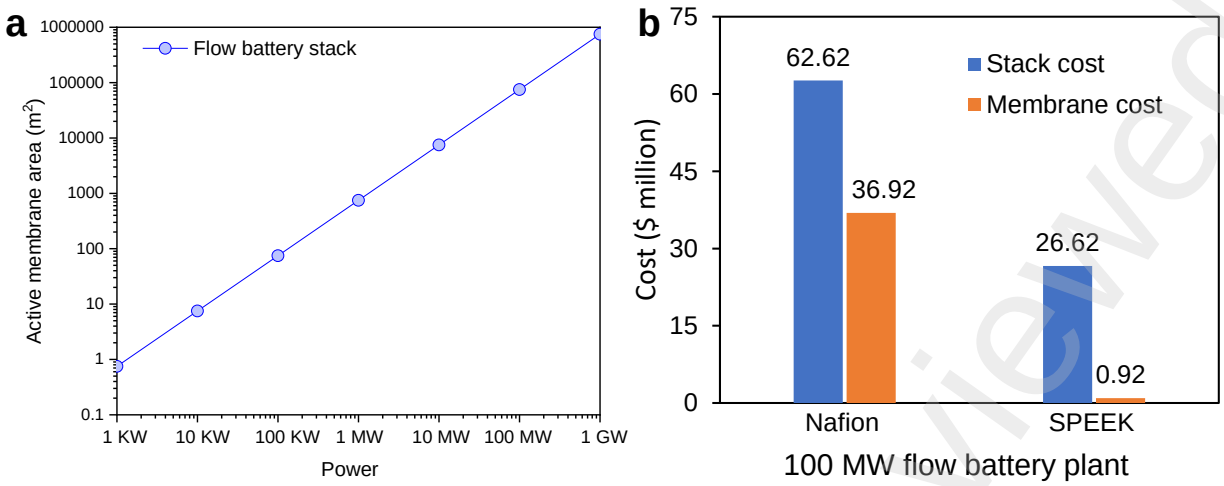
Supplementary information Table 5. The components and their costs for a 10-kW alkaline zinc-iron flow battery stack.

Component	Price per unit	Amount	Total cost ($)
Electrode	$76.92/m^2	12 m^2	923.08
Current collector	$15.38/m^2	6.2 m^2	95.38
Membrane	$12.31/m^2 (SPEEK)	7.5 m^2	92.31
	$492.31/m^2 (Nafion 212)		3692.31
Frame	$2.97/piece	60 pieces	178.15
Copper plate	$103.08/piece	2 pieces	206.15
End plate	$127.69/piece	2 pieces	255.38
Isolation plate	$193.85/piece	2 pieces	387.69
Gasket	$3.38/piece	120 pieces	406.15
O-gasket-1	$0.46/piece	232 pieces	107.08
O-gasket-2	$0.69/piece	16 pieces	11.08

Note: O-gasket-1 for current collector, O-gasket-2 for end plate.

Preprint not peer reviewed

This preprint research paper has not been peer reviewed. Electronic copy available at: https://ssrn.com/abstract=3981895



Supplementary Figure 23. Cost analysis. a, The relationship between the power of flow battery stack and the required membrane area. **b**, The stack cost and membrane cost for a 100 MW flow battery plant using different membranes.

Preprint not peer reviewed

This preprint research paper has not been peer reviewed. Electronic copy available at: https://ssrn.com/abstract=3981895

References

1 Chen, D., Wang, S., Xiao, M. & Meng, Y. Synthesis and characterization of novel sulfonated poly(arylene thioether) ionomers for vanadium redox flow battery applications. *Energy & Environmental Science* **3**, 622-628, (2010).

2 Yang, Z. *et al.* Alkaline Benzoquinone Aqueous Flow Battery for Large-Scale Storage of Electrical Energy. *Advanced Energy Materials* **8**, 1702056, (2018).

3 Wang, C. *et al.* High-Performance Alkaline Organic Redox Flow Batteries Based on 2-Hydroxy-3-carboxy-1,4-naphthoquinone. *ACS Energy Letters* **3**, 2404-2409, (2018).

4 Tong, L. *et al.* Molecular Engineering of an Alkaline Naphthoquinone Flow Battery. *ACS Energy Letters* **4**, 1880-1887, (2019).

5 Li, Y., Liu, Y., Xu, Z. & Yang, Z. Poly(phenylene oxide)-Based Ion-Exchange Membranes for Aqueous Organic Redox Flow Battery. *Industrial & Engineering Chemistry Research* **58**, 10707-10712, (2019).

6 Kwabi, D. G. *et al.* Alkaline Quinone Flow Battery with Long Lifetime at pH 12. *Joule* **2**, 1894-1906, (2018).

7 Cao, J., Tao, M., Chen, H., Xu, J. & Chen, Z. A highly reversible anthraquinone-based anolyte for alkaline aqueous redox flow batteries. *Journal of Power Sources* **386**, 40-46, (2018).

8 Lee, W., Park, G. & Kwon, Y. Alkaline aqueous organic redox flow batteries of high energy and power densities using mixed naphthoquinone derivatives. *Chemical Engineering Journal* **386**, (2020).

9 Chen, D. *et al.* Porous Membrane with High Selectivity for Alkaline Quinone-Based Flow Batteries. *ACS Applied Materials & Interfaces* **12**, 48533-48541, (2020).

10 De Porcellinis, D. *et al.* Communication—Sulfonated Poly (ether ether ketone) as Cation Exchange Membrane for Alkaline Redox Flow Batteries. *Journal of The Electrochemical Society* **165**, A1137-A1139, (2018).

11 Lin, K. *et al.* A redox-flow battery with an alloxazine-based organic electrolyte. *Nature Energy* **1**, 16102, (2016).

12 Zhang, J. *et al.* An all-aqueous redox flow battery with unprecedented energy density. *Energy & Environmental Science* **11**, 2010-2015, (2018).

13 Gong, K. *et al.* A zinc–iron redox-flow battery under $100 per kW h of system capital cost. *Energy Environ. Sci.* **8**, 2941-2945, (2015).

14 Ye, G., Janzen, N. & Goward, G. R. Solid-State NMR Study of Two Classic Proton Conducting Polymers: Nafion and Sulfonated Poly(ether ether ketone)s. *Macromolecules* **39**, 3283-3290, (2006).

15 Chen, L. *et al.* Measurement of hetero-nuclear distances using a symmetry-based pulse sequence in solid-state NMR. *Physical Chemistry Chemical Physics* **12**, 9395-9405, (2010).

16 Kusoglu, A. & Weber, A. Z. New Insights into Perfluorinated Sulfonic-Acid Ionomers. *Chemical Reviews* **117**, 987-1104, (2017).

17 Jalani, N. H. & Datta, R. The effect of equivalent weight, temperature, cationic forms, sorbates, and nanoinorganic additives on the sorption behavior of Nafion®. *Journal of Membrane Science* **264**, 167-175, (2005).

18 Mohamed, H. F. M., Kobayashi, Y., Kuroda, C. S. & Ohira, A. Effects of Ion Exchange on the Free Volume and Oxygen Permeation in Nafion for Fuel Cells. *The Journal of Physical Chemistry B* **113**, 2247-2252, (2009).

19 Xie, G. & Okada, T. The state of water in Nafion 117 of various cation forms. *Denki Kagaku* **64**, 718-726, (1996).

20 Okada, T., Arimura, N., Satou, H., Yuasa, M. & Kikuchi, T. Membrane transport characteristics of binary cation systems with Li+ and alkali metal cations in perfluorosulfonated ionomer. *Electrochimica Acta* **50**,

Preprint not peer reviewed

This preprint research paper has not been peer reviewed. Electronic copy available at: https://ssrn.com/abstract=3981895

3569-3575, (2005).

21 Yoshida, H. & Miura, Y. Behavior of water in perfluorinated ionomer membranes containing various monovalent cations. *Journal of Membrane Science* **68**, 1-10, (1992).

Preprint not peer reviewed

This preprint research paper has not been peer reviewed. Electronic copy available at: https://ssrn.com/abstract=3981895